10-19-2010

The Green and Ampt Infiltration Model Accounting for Air Compression and Air Counterflow in the Shallow Water Table Environment: Laboratory Experiments

Yuliya Lukyanets
University of South Florida

The Green and Ampt Infiltration Model Accounting for Air Compression and Air Counterflow in the Shallow Water Table Environment: Laboratory Experiments

by

Yuliya Lukyanets

A thesis submitted in partial fulfillment
of the requirements for the degree of
Master of Science in Civil Engineering
Department of Civil and Environmental Engineering
College of Engineering
University of South Florida

Major Professor: Mahmood Nachabe, Ph.D.
Mark A. Ross, Ph.D.
Kenneth Trout, Ph.D.

Date of Approval:
October 19, 2010

Keywords: Rainfall, Sharp Wetting Front, Air Entrapment Effects, Lisse Effect, Encapsulated Air

DEDICATION

I dedicate this work to my mother. Thank you for all your support throughout my academic and personal life. Thank you for your love and your care. I could not do it without you.

ACKNOWLEDGEMENTS

I would like to thank Dr. Mahmood Nachabe for his continuous guidance, support, and commitment to research. I would also like to thank Dr. Mark Ross and Dr. Ken Trout for their insights. Thank you very much to Jeffrey Vomacka for his frequent guidance and invaluable assistance throughout this research. I would also like to extend special gratitude to Jeffrey Vomacka for his help in conducting laboratory experiments that made this research possible.

TABLE OF CONTENTS

LIST OF TABLES

LIST OF FIGURES

ABSTRACT

Water infiltration into the unsaturated zone especially in a shallow water table environment is affected by air compression ahead of the wetting front and air counterflow. Neglecting air compression in infiltration modeling can overestimate infiltration and infiltration rates, whereas not accounting for air counterflow can underestimate infiltration and infiltration rates due to unrealistic buildup of air pressure resistance ahead of the wetting front. A method, derived on the basis of the Green and Ampt (1911) infiltration model, is introduced to simulate air compression and air counterflow during infiltration into a shallow water table. The method retains the simplicity of the Green and Ampt (1911) model but adds the air pressure resistance term ahead of the wetting front. Infiltration equations are derived on the basis of the Green and Ampt (1911) and Sabeh's (2004) infiltration model which accounts for air compression and air counterflow. The difference between this method and Sabeh's (2004) model is that air counterflow, air compression, and infiltration are decoupled and updated with each wetting front increment whereas Sabeh's (2004) method uses time step as a decoupling mechanism. Air compression ahead of the wetting front is predicted using the perfect gas law.

Laboratory experiments showed that the introduced method is reasonably accurate when modeling cumulative infiltration values. Results of laboratory experiments were

compared to results of the modeled infiltration methods: original Green and Ampt (1911) model and Green and Ampt with air compression and counterflow.

The advantage of this new method is its simplicity. The new method uses parameters that are generally needed for modeling infiltration with the Green and Ampt (1911) approach. Disadvantages of the model are assumptions of the uniform water content and the uniform pressure. Another shortcoming of the model is that it does not account for air compression and air counterflow prior to ponding.

Laboratory experiments described in this work and a proposed model can be further used for modeling and studying infiltration with air effects. In addition, this work can be of use to someone studying irrigation techniques of rice or other crops.

CHAPTER 1: INTRODUCTION

1.1 Background

A classic problem in hydrology and soil science is the prediction of cumulative infiltration and infiltration rates in unsaturated soils. Infiltration and infiltration rates affect water economy, surface runoff, and development of erosion (Hillel 1982). Prediction of infiltration is paramount for determining runoff rates and developing stormwater routing models. Infiltration components of runoff modeling have been studied for decades; however, due to the complexity of the infiltration process represented in runoff modeling, a universally accepted method of calculating infiltration does not exist. The Green and Ampt (1911) model has received widespread attention in recent years as a simple model more or less describing the primary mechanisms of gravity and suction flow (Charbeneau 2000). However, in engineering practice a professional must apply his knowledge of modeling, experience, and availability of data to estimate model parameters and infiltration (Durrans et al. 2007).

However, the Green and Ampt (1911) model does not account for soil air compression or air counterflow. Recent research has focused on the effects of air on infiltration rates and cumulative infiltration (Touma et al. 1984, Faybishenko 1995, Wang et al. 1997, Seymour 2000, Sabeh 2004). Experimental results have shown that it is

problematic to ignore air compression and air counterflow especially in shallow water table environments, where air has no place to escape but upwards. Recent research shows that air entrapment occurs under intense rain (Hammecker et al. 2003).

Although being very similar to Sabeh's (2004) conceptual model, the revised Green and Ampt infiltration model, presented in this work, updates air pressure by calculating air flux and remaining air volume at every wetting front depth increment ΔL. This differs from Sabeh's (2004) model. In addition, in this paper experimental results from laboratory experiments, dealing with air entrapment ahead of the wetting front and air counterflow, are presented and compared to the modeled results.

1.2 Objectives and Scope

The purpose of this research is to develop a modification of a popular infiltration model, the Green and Ampt (1911) model. It is known that one-dimensional water movement computer programs, such as Hydrus-1D, cannot simulate air effects on infiltration (Simunek et al. 1998, Hammecker 2003).

It is important to emphasize that the basis for the introduced modified Green and Ampt infiltration model is Sabeh's (2004) infiltration model, known as MODGA. Sabeh's (2004) model accounts for air compression and air counterflow in porous media by calculating volume occupied by air at every time increment Δt. Unlike MODGA (Sabeh 2004), the introduced modified Green and Ampt (1911) model updates the volume occupied by air at every wetting front depth increment ΔL. The primary objective of the introduced model is to improve estimates of cumulative infiltration by accounting

for air compression and air counterflow while retaining the simplicity of the Green and Ampt (1911) infiltration model.

An overview of this thesis is as follows: CHAPTER 1 offers background information on the original Green and Ampt (1911) infiltration model; discusses effects of air compression and air counterflow on infiltration; reviews other well-known infiltration models; and introduces recent similar studies. CHAPTER 2 describes the materials and methods, used in this research, and describes the soil column experiments. CHAPTER 3 describes the introduced infiltration model. CHAPTER 4 presents the results of the proposed infiltration model. Finally, CHAPTER 5 discusses successes and shortcomings of this research, summarizes important conclusions of this study and offers suggested improvements in future studies.

1.3 Influence of Air on Infiltration

Research shows that water infiltration into the soil is affected by air compression ahead of the wetting front and air counterflow. Since the proposed model couples air compression and air counterflow with infiltration, this section will discuss effects of air compression and air counterflow on infiltration and will offer a summary on air entrapment.

1.3.1 Effects of Air Compression and Air Entrapment

Effects of air compression, also known as air confinement ahead of the wetting front, have been studied by many researchers in the field of hydrology and soil science (Touma et al. 1984, Wang et al. 1997, Seymour 2000, Dunn et al. 2003). It was believed that effects of air compression on infiltration were insignificant. In addition, air pressure of soil air was assumed to be atmospheric since scientists believed that air escaped freely once water infiltrated through the soil (Wang et al. 1997). Wang et al. (1997) derived an analytical model accounting for air compression, air counterflow, and hysteresis based on the Green and Ampt (1911) infiltration model. Similar to this thesis, Wang et al. (1997) calculated air compression using the perfect gas law. Wang et al. (1998) measured air pressure ahead of the wetting front as "the simultaneous changes in the rates of water inflow and air outflow." They found out that air pressure increased with time, in the conditions when air had nowhere to escape but upwards (Wang et al. 1998). Wang et al. (1998) also found that maximum air pressure ahead of the wetting front was reached when air started erupting from the soil surface or when bubbling occurred on the surface of the soil. Moreover, Wang et al. (1998) came up with empirical equations to predict maximum air pressure ahead of the wetting front.

In addition, research show that effects of air entrapment on infiltration cannot be ignored. Seymour (2000) tested affects of air entrapment on hydraulic conductivity in a 50 mm soil sample. Izadi (1995) showed that air entrapment, described as a 10% decrease in the rewet water content, reduced cumulative infiltration by 21%. Klute (1973) indicated that 25% of the available porosity can be entrapped by air bubbles when wetting a sandy soil column to natural saturation. Seymour (1990) conducted a lab

experiment and showed 10.5% reduction in the rewet water content of the sandy soil due to air entrapment caused by intermittent application of water. Touma et al. (1984) conducted an experiment on the 93.5 cm high soil column and found out that air entrapment caused reduction of water intake by a significant factor of 2.5. Peck (1969) wrote about air entrapment effects on soil moisture content and Hillel (1982) listed a decrease in water content, due to entrapped air, as one of the reasons behind hysteresis. It is important to note that it is believed that air entrapment occurs in the first few centimeters of soil (Seymour 2000).

This section would not be complete without mentioning a rare hydrologic phenomenon of the Lisse effect first observed by Thal Larsen in 1932, while conducting well studies in the village of Lisse in Holland, known for its dune sands and shallow water table (Weeks 2002). Larsen noted that under conditions of high intensity rainfall, compressed air in front of the advancing wetting front causes an abrupt rise in the water table, although the wetting front has not yet reached the water table (Weeks 2002). Larsen determined that the rise in the water table was not attributed to soil moisture reaching the water table but rather to compressed air ahead of the wetting front pushing on the water table (Weeks 2002).

According to Weeks (2002), the Lisse effect is a rare phenomenon which does not occur in all field conditions but only in ideal circumstances: in shallow water table environments and in wells screened below the water table. My experimental results support Weeks' findings. Out of the first four soil column experiments, conducted under ponded conditions and in the shallow water table environment, only the first two experiments showed the Lisse effect captured by well data loggers. My speculation is that

a combination of the initial soil moisture, the amount of compressed and entrapped air causes the occurrence of the Lisse effect. Since with each subsequent experiment the amount of entrapped air in the soil can diminish due to the dissolution of air, the Lisse effect may not be observed in the subsequent experiments.

After Larsen's discovery, several scientists and researchers described the Lisse effect after observing the phenomenon in field and laboratory settings (Meyboom 1967, Hughs et al. 1971, Heliotus and De Witt 1987). Occurrence of the Lisse effect was also noted and described in a more recent study by Vomacka et al. (2002). The study was conducted in Lithia, Florida (Vomacka et al. 2002). The abrupt rise of the water table was recorded by a well pressure transducer despite the fact that at that time the change in soil moisture was not yet recorded anywhere near the water table (Vomacka et al. 2002). The abrupt rise was due to "a pressure gradient between the compressed air in the vadose zone and the air in the monitoring well" (Sabeh 2004).

A recent study of the flow of water in a shallow water table environment and under irrigation conditions was conducted in northern Senegal (Hammecker et. al 2003). The results of the study showed that the air entrapment between the wetting front and the shallow water table reduced infiltration rates (Hammecker et al. 2003).

1.3.2 Effects of Air Counterflow on Infiltration

Powers (1934) and Free and Palmer (1940) were among the first investigators who observed air bubbles escaping through the soil surface during irrigation practices (Youngs and Peck 1964). Youngs and Peck (1964) wrote that air could escape as air

bubbles through the soil surface once pore pressure forces were large enough to overcome the forces at the water-air interface. Unfortunately they did not provide any insight on what pressure it took for air, enclosed between the advancing wetting front and the "water-saturated material" (water table), to escape in form of air bubbles through the soil surface (Youngs and Peck 1964). As mentioned earlier, Wang et al. (1998) found that maximum air pressure ahead of the wetting front occurred at the same time that bubbling occurred.

Tindall et al. (1999) found that during ponded surface and near-saturation conditions air counterflow was hindered by "a viscous resistance," developed behind the advancing wetting front, which reduced infiltration rates.

1.4 Review of Existing Literature

This section is devoted to description of the common infiltration definitions, infiltration processes, and known infiltration models.

1.4.1 Problem of Terminology

Since the main purpose of this study is modeling of infiltration, the study cannot be complete without a description of some of the definitions commonly used when describing infiltration processes. Infiltration rate is defined as "the volume flux of water flowing into the profile per unit of soil surface area per unit time" (Hillel 1982). There appears to have been some discussion among scientists on what should have been a

proper term for the infiltration rate once the rainfall rate exceeds the ability of the soil to absorb water. Horton (1940) called this rate "infiltration capacity. " Richards (1952) pointed out that the term "infiltration capacity" implied a rather "extensive aspect" of the soil ability to absorb water and hence was confusing. I also believe that the term "infiltration capacity" creates some confusion particularly among scholars new to the study of hydrology and infiltration. When Horton (1940) coined the term he referred to the maximum rate at which infiltration could proceed once ponding was attained (Hillel 1982). Hillel (1982) argued that infiltration rate could exceed "infiltration capacity" if the ponding depth at the surface was substantial. Although the term "infiltrability" coined by Hillel in 1971 appears to be more appropriate and less confusing to describe "the infiltration flux resulting when water at atmospheric pressure is freely available at the soil surface," the term did not adapt well in literature (Hillel 1982). Hence, I will abstain from using the term "infiltrability" and use the term "infiltration capacity" to describe maximum infiltration rate once ponding is reached at the soil surface. The term "infiltration capacity" is the most widely accepted in soil-water modeling.

It is also worth noting a difference between air compression and air entrapment, two terms that are often confused and used interchangeably in scientific literature. Faybishenko (1995) recognized the problem of terminology in infiltration studies that describe water movement in air-water interface and made a clear distinction between air compression and air entrapment. Faybishenko (1995) defined entrapped air as the "air surrounded by water in the porous space of soils." He described compressed air as the "air compressed ahead of the wetting front" (Faybishenko 1995). Similar to Faybishenko (1995), Youngs and Peck (1964) wrote that air entrapment occurs when " ….smaller air

pockets are entrapped in the centers of soil crumbs which are surrounded by saturated larger pores." Interestingly, Faybishenko (1995) modeled entrapped air under conditions of ponded infiltration, conditions under which air compression (with air counterflow) were modeled in this study. In this study I will refer to the air compressed ahead of the wetting front as air compression.

1.4.2 Infiltration Models

Infiltration models vary in their complexity and sophistication since the infiltration process is difficult to characterize due to highly variable initial conditions and soil properties (Viessman and Lewis 2003). Considerable research has been done in the area of infiltration and stormwater runoff; however, no single equation or mechanism can portray all infiltration scenarios (Viessman and Lewis 2003). The assumptions are the key components in understanding a particular infiltration model. Most of the infiltration studies can be divided into studies that deal with empirical equations based on field or laboratory observations and studies that deal with solutions of equations based on Darcian flow in porous media often referred to as physically-based equations. This chapter reviews some of the most widely applied infiltration models, both empirical and physically-based, and presents them in their historical order. The earliest infiltration equation was introduced by Green and Ampt in 1911 (Hillel 1982), but we will reserve the discussion of this empirically based infiltration equation and its numerous versions to the last. Discussion of the Green and Ampt (1911) equation is presented in the following section.

One of the earliest infiltration models is the one proposed by the Russian scientist A.N. Kostiakov (Hillel 1982). Kostiakov (1932) proposed an empirical infiltration equation:

$$F = at^b, \qquad \text{Equation 1}$$

where a and b are constants and ($0 < b < 1$) (Mishra et al. 2003). Rode (1965) differentiated Equation 1 and modified Kostiakov infiltration equation to obtain an equation for the infiltration rate in the form of:

$$f = \alpha(t)^{-\beta}, \qquad \text{Equation 2}$$

where $\alpha = ab$ and $\beta = 1-b$ are determined experimentally (Mishra et al. 2003). Hillel (1982) pointed out that, while simple in its form, Equation 2 can be relevant for "purely horizontal water absorption and is deficient for downward infiltration." Smith (1972) modified Kostiakov infiltration equation to include a constant nonzero infiltration rate f_c:

$$f = f_c + \alpha(t)^{-\beta}. \qquad \text{Equation 3}$$

It is important to note that f_c is the asymptotic steady constant infiltration rate reached when t and F are large.

Hortonian, or infiltration excess runoff (Horton 1939) and Dunne runoff, or saturation excess (Dunne and Black 1970) remain the two widely recognized surface runoff mechanisms in hydrology and soil science. Hortonian, or infiltration excess runoff occurs when rainfall or irrigation intensity exceeds the infiltration capacity. Runoff begins when the soil surface reaches saturation and infiltration proceeds at its capacity which is less than the rainfall rate. In contrast, the second mechanism, known as

saturation excess runoff, begins when infiltration water fully saturates the soil profile above a shallow water table or an impervious surface, resulting in cessation of infiltration (Nachabe et al. 2004).

Horton (1939) developed an empirical equation for determining infiltration capacity. Horton developed this equation to describe an exponential decay of infiltration rate with time (Durrans et al. 2007). Although simple in its form, Horton's infiltration capacity equation is limited in its use due to difficulty in determining values of f_0 and k which depend upon soil type and vegetative cover (Durrans et al. 2007):

$$f(t) = f_c + (f_0 - f_c)e^{-k(t-t_0)}, \qquad \text{Equation 4}$$

where:

- $f(t)$ = infiltration capacity or infiltration rate at some time t,
- k = a constant representing the rate of decrease in f,
- f_c= a final or equilibrium capacity or final infiltration rate,
- f_0= the initial infiltration capacity.

Cumulative infiltration can be found by integrating Equation 4 and applying initial conditions (Tindall et al. 1999):

$$I = f_c t + \frac{(f_o - f_c)}{k}(1 - e^{-kt}). \qquad \text{Equation 5}$$

The Philip model (1957) is a physically-based infiltration model and it is widely used in the field of irrigation. Philip (1957), after publishing a series of papers on

cumulative infiltration in a horizontal soil and coining the term sorptivity provided a vertical infiltration equation (Mishra et al. 2003):

$$F = St^{1/2} + At, \qquad \text{Equation 6}$$

where:

- F = cumulative infiltration,
- S = sorptivity,
- A = soil parameter .

Equation 6 is applied to vertical infiltration with ponding water on top of the soil column. Philip (1957) defined sorptivity as a soil parameter dependent on soil properties and provided an approximate solution for sorptivity for infiltration in a horizontal soil column in the form of:

$$S = \frac{(\theta_s - \theta_i)x}{t^{1/2}}, \qquad \text{Equation 7}$$

where θ_s and θ_i are the saturated and initial water content and x is the length of the horizontal wetting front. However this approximation of sorptivity cannot be used in Equation 6 since it has been developed for a horizontal soil column. Hence, regression techniques as well as experimentally based approximations of Rawls et al. (1983) and Youngs (1964) can be used to estimate sorptivity S (Tindall et al. 1999). Rawls et al. (1983), and Youngs and Peck (1964) also developed approximations for the soil parameter A. In the Phillip (1957) equation A is the soil parameter that is related to soil

hydraulic conductivity and similar to K_s for saturated conditions (Tindall et al. 1999). By differentiating Equation 6 vertical infiltration rate equation can be obtained:

$$f = \tfrac{1}{2} St^{-1/2} + A. \qquad \text{Equation 8}$$

As Equation 8 suggests, after a long period of time t, infiltration rate f becomes the soil parameter A that at a large t should equal saturated hydraulic conductivity K_s.

Holtan (1961) developed an empirical infiltration equation, first introduced in 1961 (Tindall et al.1999). The Holtan (1961) model accounts for the unfilled capacity of the soil to store water (Tindal et al. 1999) and it is in the form of:

$$f = a(M - I)^n + f_c, \qquad \text{Equation 9}$$

where a and n are constants, dependent on the soil type, surface and cropping conditions, and *(M-I)* is the "unfilled capacity of the soil to store water" or potential infiltration (Tindall et al. 1999) with M defined as the porosity minus the antecedent soil moisture (Mishra et al. 2003). In 1975 Holtan introduced the growth index G of the vegetative cover and modified the initially proposed infiltration equation to account for the effect of vegetation (Mishra et al. 2003). Huggins and Monke (1966) modified the Holtan (1961) model by introducing the porosity ϕ in the denominator:

$$f = \frac{a(M - I)^n}{\phi^m} + f_c. \qquad \text{Equation 10}$$

where m is another empirical parameter.

Of the above presented conventional infiltration models only the Philip (1957) model is reportedly more physically-based.

Overton (1964) model is a less known infiltration model. Overton (1964), using the Holtan (1961) infiltration model, developed the following equation:

$$f = f_c \sec^2 (af_c)^{1/2} (t_c - t) . \qquad \text{Equation 11}$$

where a is a constant and t_c is a time parameter.

Smith and Parlange (1978) developed linear and non-linear infiltration models that deal with two extreme cases of unsaturated hydraulic conductivity. These infiltration models are physically based and similar to the Philip (1957) and the Green and Ampt (1911) infiltration models emerged from infiltration theories (Hillel 1982). The Smith and Parlange (1978) linear infiltration model assumes that K varies slowly near saturation:

$$f = K_s (1 + \frac{S}{K_s I}), \qquad \text{Equation 12}$$

where S is the sorptivity and K_s is the saturated hydraulic conductivity. In contrast, the Smith and Parlange (1978) non-linear infiltration model assumes that K varies exponentially near saturation:

$$f = \frac{K_s e^{\frac{IK_s}{S}}}{e^{\frac{IK_s}{S-1}}} . \qquad \text{Equation 13}$$

1.4.3 Green and Ampt Infiltration Model Accounting for Air Compression and Air Counterflow

This section begins with a discussion of the original Green and Ampt (1911) infiltration model. The discussion of the Green and Ampt (1911) based infiltration models that account for air effects, follows.

The Green and Ampt (1911) equation is a physically-based infiltration equation that has been extensively studied and used to simulate infiltration. Green and Ampt (1911) derived the model by "applying Darcy's law to the wetted zone in the soil" (Mein and Larson 1971). The Green and Ampt (1911) equation has also been adapted for modeling infiltration through layered soils but only in soils with decreasing permeability or where water moves from coarser soil into finer less permeable soil (Chu and Marino 2005).

The Green and Ampt (1911) infiltration model is based on the assumption that "the soil may be regarded as a bundle of tiny capillary tubes, irregular in area, direction, and shape" (Mishra et al. 2003). Other assumptions include piston flow, distinct sharp wetting front, homogenous deep soil with uniform initial water content and ponded surface on top of the soil, also known as ponded head (Mishra et al. 2003).

Applying Darcy's law to the wetted zone in the soil and neglecting a pool of water on top of the soil surface, the Green and Ampt (1911) can be derived into the following infiltration equation:

$$f = \frac{dF}{dt} = K_s \frac{H_c + L}{L}, \qquad \text{Equation 14}$$

where:

- L = distance from the soil surface to the wetting front depth,
- H_c = capillary suction head at the wetting front,
- K_s = conductivity of the wetted zone.

From continuity:

$$F = (\theta_s - \theta_i)L, \qquad \text{Equation 15}$$

where θ_s and θ_i are the water content at saturation and the initial water content respectively. Substituting this relationship into Equation 14 gives:

$$f = \frac{dF}{dt} = K_s\left(1 + \frac{H_c(\theta_s - \theta_i)}{F}\right). \qquad \text{Equation 16}$$

It has been previously suggested that effects of air compression and air counterflow cannot be neglected when modeling infiltration, especially when dealing with soils under ponded conditions in a shallow water table environment (Sabeh 2004). This section describes the work of Morel-Seytoux (1973), Wang et. al (1997) and Hammecker (2003), who modified the original Green and Ampt (1911) infiltration equation to account for air compression and air counterflow.

Extending the Green and Ampt (1911) method to include air effects on infiltration, Morel-Seytoux (1973) proposed the following model:

$$f = \frac{dF}{dt} = K_s\frac{H_0 + H_c + L - H_a}{L}, \qquad \text{Equation 17}$$

where:

- f = infiltration rate [m/hr];
- t = time [hr],
- K_s = hydraulic conductivity at saturation [m/hr],
- H_0 = ponded water depth at the soil surface [m],
- H_c = effective capillary pressure head at the wetting front [m of water] also known as the soil suction head,
- H_a = gage air pressure head [m of water] immediately below the wetting front,
- L = depth to a sharp wetting front [m].

It is important to note that Morel-Setoux (1973) was one of the first to recognize the effects of air compression on infiltration (Tindall et al. 1999). Morel-Seytoux and Khanji (1974) recognized that the Green and Ampt (1911) model could overpredict infiltration by as much as 70% due to air effects (Tindall et al. 1999). Morel-Seytoux and Khanji (1974) suggested dividing K_s by β, a viscous correction factor, to account for the entrapped air in the soil (Tindall et al. 1999).

The future Green and Ampt based infiltration models accounting for air effects were based on the works of Morel-Seytoux and Khanji (1974). The challenge for the future infiltration models was to accurately account for effective capillary pressure head, H_c. H_c is a parameter that can vary significantly across the wetting front and many

investigators tried to come up with a practical way to estimate H_c to include in the modified Green and Ampt equation. Similar efforts were made to estimate the gage pressure head ahead of the wetting front H_a. Peck (1965) speculated that the gage air pressure to initiate air bubbles, bubbling pressure head, can be equal to "the water pressure at the bottom of the depth of the saturated zone plus the air entry pressure of the material" (Wang et al. 1997). Wang et al. (1997) confirmed Peck's findings and found two extremes of the gage air pressure values: air-breaking value H_b and air-closing value H_c :

$$H_b = H_0 + L + H_{ab}, \qquad \text{Equation 18}$$

$$H_c = H_0 + L + H_{wb}, \qquad \text{Equation 19}$$

where H_{ab} is the air-bubbling air pressure and H_{wb} is the water-bubbling pressure (Wang et al. 1997). Wang et al. (1997) defined H_{ab} and H_{wb} at inflection points of $d^2 S_w / dh_c^2 = 0$ of the van Genuchten (1980) model where h_c^* is the inflection capillary pressure head, S_w^* is the inflection water saturation, and α, m, and n are the van Genuchten (1980) model parameters:

$$h_c^* = \frac{1}{\alpha}\left[\frac{n-1}{n(m+1)-n+1}\right]^{1/n} = \frac{1}{\alpha} m^{1/n} \qquad m = 1 - 1/n, \qquad \text{Equation 20}$$

$$h_c^* = \frac{1}{\alpha}\left[\frac{n-1}{n(m+1)-n+1}\right]^{1/n} = \frac{1}{\alpha} \qquad m = 1 - 2/n, \qquad \text{Equation 21}$$

$$S_c^* = \left[1 - \frac{n-1}{n(m+1)}\right]^m = \left(\frac{1}{1+m}\right)^m \qquad m = 1 - 1/n, \qquad \text{Equation 22}$$

$$S_c^* = \left[1 - \frac{n-1}{n(m+1)}\right]^m = 0.5^m \qquad m = 1 - 2/n. \qquad \text{Equation 23}$$

As can be seen, this method of estimating gage air pressure head below the wetting front and suction head, is complex and requires estimation of many additional empirical parameters. Other methods to estimate suction head and gage air pressure were proposed. Bouwer (1964) proposed replacing suction head H_c with a critical pressure head, P_c (Wang et al. 1997):

$$P_c = \frac{1}{K_s}\int_0^{\infty} K_{rw}\, dH_c, \qquad \text{Equation 24}$$

where K_s is the saturated hydraulic conductivity and K_{rw} is the relative hydraulic conductivity and is equal to K/K_s (Wang et al. 1997).

An easier method of estimating a critical pressure head P_c to obtain the effective capillary pressure head H_c was proposed by Morel-Seytoux et al. (1996):

$$P_c = \frac{0.046m + 2.07m^2 + 19.5m^3}{\alpha\left(1 + 4.7m + 16m^2\right)}. \qquad \text{Equation 25}$$

In contrast, Whisler and Bouwer (1970) suggested that capillary pressure head H_c is the air entry pressure in the Brooks and Corey (1966) retention model. Morel-Seytoux and Khanji (1974) proposed replacing the capillary pressure head H_c in the modified Green and Ampt equation by the effective capillary drive H_{ef}:

$$H_{ef} = \int f_w dH_c ,$$ Equation 26

where f_w is the "fractional flow function accounting for the relative water conductivity, K_{rw}, and the relative air conductivity, K_{ra}" (Morel-Seytoux and Khanji 1974). In addition, instead of K_s they used K_s/β where β is the "viscous resistance correction factor" (Morel-Seytoux and Khanji 1974).

Later Brakenseik (1977) proposed a simplified method of calculating the effective capillary pressure H_c which Brakensiek called S and proposed calculating as:

$$S = \frac{2+3\lambda}{1+3\lambda} H_c ,$$ Equation 27

where λ is the pore size distribution index in the Brooks and Corey (1966) retention model .

Extending the Green and Ampt (1911) approach further, Wang et al. (1997) formulated infiltration equations accounting for air compression, air counterflow, and hysteresis effects. They assumed homogenous soil profile and a sharp wetting front (Wang et. al 1997). For periods of air compression and when H_a is less than air-closing value, $H_c = L+H_0+H_{wb}$, Wang et al. (1997) used:

$$f = K_c \frac{L + H_0 + H_{wb} - H_a}{L} ,$$ Equation 28

where $Ks=k_{rc}K_s$ and k_{rc} is the relative water conductivity.

For periods of air counterflow Wang et. al (1997) used:

$$f = \frac{K_c(H_{ab} - H_{wb})}{2}\left[z_0^2 + K_c(H_{ab} - H_{wb})(t - t_0)\right]^{-1/2}, \quad \text{Equation 29}$$

Wang et al. (1977) also developed an explicit equation for the entire infiltration period that consists of the period with air compression ahead of the wetting front followed by the periods with air counterflow:

$$f = \frac{1}{2}\left[K_c\phi\left(1 - S_{w,0} - S_{nw,c}\right)\left(H_{ab} - H_{wb}\right)\right]^{1/2} t^{-1/2}. \quad \text{Equation 30}$$

where $S_{w,0}$ is the initial water saturation before infiltration and $S_{nw,c}$ is the residual air entrapment under air-confining conditions (Wang et al. 1977). It is intuitive that the infiltration rate as defined by the above equation "does not reach a constant value, but continuously decreases with the square root of time (Hammecker et al. 2003).

Similar to Wang et al. (1997), Hammecker et al. (2003) proposed two-phased infiltration equations on the basis of the Green and Ampt (1911) method but used a slightly different approach. Hammecker et al. (2003) tested the results of their proposed model on the rice fields of northern Senegal, "where rice was grown under flood irrigation, and a superficial pond of 5-25 cm was maintained during the complete plant growth cycle (about 100 days)." Under conditions of ponded head that exceeded 20 cm, air compression effects on infiltration rates were found to be paramount (Hammecker et al. 2003).

Similar to Wang et al. (1997) Hammecker et al. (2003) used Boyle's law to calculate air pressure:

$$H_a = H_{atm}(\frac{L}{D-L}), \qquad \text{Equation 31}$$

where H_{atm} is the atmospheric air pressure (≈ 10 m of water). As Equation 31 suggests the shallower the water table depth D is, the higher the air pressure H_a for specific wetting front depth L. However, the effect of decreasing water table on increase in air pressure is not as abrupt in comparison on how air pressure reacts to even a slight increase in the wetting front depth. For instance, 0.01 meter change in the wetting front doubles the air pressure for a given water table depth.

In "Experimental and Numerical Study of Water Flow in Soil under Irrigation in Northern Senegal: Evidence of Air Entrapment," Hammecker et. al (2003) argues the applicability of Wang et. al (1997) equation that describes the entire period of infiltration rate. Hammecker et al. (2003) questions the cyclical nature of the Wang et al. (1997) equation when dealing with air pressure. Hammecker et al. (2003) mentions numerous experimental studies show that air pressure eventually reaches a maximum constant value during infiltration. Experimental studies in this thesis suggest cyclical nature of air pressure. It is reflected in the behavior of infiltration rates observed during lab experiments. However, the proposed model simulates a continuously increasing gage air pressure which is, when achieved, shuts off infiltration.

1.5 Contribution of the Study

As mentioned earlier, for the experimental validation of the proposed model several soil column experiments were conducted. Soil column experiments involved

simulating instantaneous air compression ahead of the wetting front (as during a high intensity rainfall event) by pouring a large amount of water on top of the soil column. In these experiments a constant pressure head was rapidly achieved by pouring water on top of the soil column and maintained using water pumps. In addition a number of experiments were carried out using a constant pressure head that was gradually achieved by pouring water through a garden hose water nozzle with a “rainfall-like” showerhead.

CHAPTER 2: MATERIALS AND METHODS

2.1 Experimental Setup

The experimental setup composed of the three-dimensional (3-D) soil column, water main, well, tensiometers, soil moisture sensors, and data loggers.

2.1.1 Soil Column Description

A three-dimensional column (square inner diameter of 45.7 cm and soil height of 180.34 cm), constructed of transparent Plexiglass acrylic sheets and open at the top and closed at the bottom and sides, was used in the laboratory experiments. The bottom of the soil column was filled with porous air transmission stones and the column was positioned on the steel plate. The column was also equipped with a well to capture water level fluctuations and with a scale, accurate to 0.23 kg, to measure weight changes of the soil column . Description of the well can be found in Measurement Setup section. The column had no lateral openings other than those for soil moisture sensors and tensiometers and was only open at the top (see Measurement Setup section). Experimental setup of the soil column is depicted in Figure 1.

Figure 1: Experimental Setup

2.1.2 Soil Characterization

Soil used in soil column experiments was somewhat typical of the West-central Florida soils. The vertical soil column was filled with sand graded from 0.07 mm to 1.2 mm, with 92% of soil being less than or equal to 0.5 mm (3.5% of 20-30 graded sand, 30% of 30-65 graded sand, 17.5 % of 50-140 graded sand, and 49% of 70-200 graded sand). The sand, after being carefully poured into the transparent 3-D column, was compacted with the standard proctor hammer (30 blows per every 20 cm of sand).

2.1.3 Permeability Tests

To measure natural saturated hydraulic conductivity, K_{ns} (also known as permeability) of the soil used in the soil column experiments, several constant head permeability tests were conducted separately from the main soil column experiments. Constant head permeability tests were conducted on a smaller sand sample. The mold (cylinder inner diameter of 10.2 cm and soil height of 11.43 cm) was filled with sand used in the 3-D soil column and compacted using the same compaction method implemented in the experimental setup. After compaction the bulk density was measured to be 1.61 g/cm^3. Note that this number (1.61 g/cm^3) is representative of the average bulk density in the 3-D column and not an exact value. This is due to the fact that constant head permeability tests and bulk density tests were conducted on the soil sample much smaller than the experimental setup soil sample. Although the soil, used for the permeability tests' smaller sample, was compacted using similar packing method, compaction of the 3-D soil column was not exactly replicated. It is difficult to achieve same compaction on a soil sample, which is 15 times smaller than the experimental setup sample. The same compaction might have been achieved by carefully removing the soil sample from each 10 cm layer of the 3-D soil column and taking measurements on every 10 cm-layer. However, this could have disrupted the 3-D soil column's natural layers.

A number of constant head permeability tests indicated that the average saturated hydraulic conductivity, K_s of the sand was 322 cm d^{-1} (13.42 cm hr^{-1}, 3.73 x 10-5 m s^{-1} , or 2.2 mm min^{-1}). As for the bulk density number (see discussion above), natural saturated hydraulic conductivity of the sand sample is just a representative value of the natural saturated hydraulic conductivity K_{ns} of the 3-D column soil and is not an exact

match. In algorithm simulations (see CHAPTERS 3 and 4) K_{ns} = 10 cm hr^{-1} was used. K_{ns} of 13.42 cm hr^{-1} was initially used as a fitting parameter in the introduced model but produced a poor match of observed and modeled values.

2.2 Data Collection and Measurement Setup

The measurement setup was composed of tensiometers, soil moisture sensors, and data loggers.

2.2.1 Tensiometers

Pressures were measured using typical tensiometers (pressure–sensing devices and porous elements inserted into the soil). Tensiometers were tested and described by numerous researchers and are well described by Charbeneau (2000). Ten tensiometers at depths of 30, 40, 50, 60, 70, 80, 90, 100, 110, and 120 cm relative to the bottom of the soil column were used in the soil column experiments. The pressure sensors used in the tensiometers were Honeywell pressure sensors with scan rate of 5 seconds, log rate of 2 minutes, sensing range of 1.0 psi - 250 psi, and accuracy of 0.25%. During each experiment, signals from pressure transducers were recorded at 2min intervals using Starlog 4 data logging and management software. Tensiometers were tested for accuracy prior to the soil column experiments. Pressure values were recorded every two minutes in the first series of soil column experiments and every minute in the subsequent soil column experiments.

Pressure readings recorded by tensiometers allowed to capture pressure fluctuations and allowed to focus on pressure abrupt rises during the experiment and to capture gage air pressure that we were interested in.

2.2.2 Soil Moisture Sensors

Water contents were measured using sixteen soil moisture sensors. Water contents were measured using EnviroSCAN® soil moisture probes (available from Sentek, Adelaide, Australia) inserted into the soil column within 10 cm of each other along the soil column height. Water contents were measured at z =8.5, 18.5, 28.5, 38.5, 48.5, 58.5, 68.5, 78.5, 88.5, 98.5, 108.5, 118.5, 128.5, 138.5, 148.5, and 158.5 cm ($z=0$ cm is at the soil column surface; the axis is positively downward). Soil moisture readings were recorded every two minutes in the first series of soil column experiments and every minute in the subsequent experiments.

Measuring the actual infiltration depth during rainfall is challenging because water content changes rapidly close to the land surface as the wetting front propagates downward. The advantage of the EnviroScan® technology is that multiple sensors allow for continuous monitoring of water content evolution with time from land surface to 1.5 m. At each depth listed above, the sensor provided data over a 10 cm average depth at two minutes intervals. The sensors use the principle of electrical capacitance (frequency-domain reflectometry) and are expected to provide volumetric water content ranging from oven dryness to saturation with a resolution of 0.1%. These sensors were tested by a number of investigators (Charbeneau 2000).

2.2.3 Data loggers

In addition, a continuously recording water level data logger was used to measure the depth to the water table every two minutes. The well (made of 5.08 cm in diameter PVC pipe) housed the Solinst® Levelogger® Gold submersible water level data logger that included a pressure transducer and a temperature sensor. The Solinst® Levelogger® pressure transducer uses infra-red data transfer and is accurate to 0.05%. The well had a total depth of approximately 1.5 m. The well was screened below the water table to allow the pressure transducer to record the Lisse effect, the pressure of the air phase pushing on the water table during infiltration. Since Solinst® Levelogger® data logger measured absolute pressure, Solinst® Barologger® was used to compensate for atmospheric pressure fluctuations by measuring barometric pressure also recorded every two minutes.

2.3 Description of Infiltration Experiments

Eleven experimental studies were conducted on a vertical 3-D soil column to test an Excel algorithm of a simple set of infiltration equations (see CHAPTER 3). Experiments were conducted in the soil column that was laterally sealed except for the openings intended for tensiometers and soil moisture sensors. Hence, pressure readings captured during the experiments were associated with bursts of air trying to escape through the soil column surface as water infiltrated and propagated to deeper layers of soil .

All experiments were run at a temperature of 20˚C (see Appendix A for water and air properties). Hydrostatic pressure conditions were reached between the experiments.

Prior to each experiment, melted petroleum jelly was applied to seal the periphery of the soil column (between the sand and the Plexyglass sheets of the 3-D column) to avoid development of cracks along the walls of the soil column and fingering.

Experiments were carried out for one infiltration condition: air was confined in the soil column. First four experiments were conducted using a constant pressure head that was instantaneously achieved by pouring water on top of the soil column and maintained using water pumps. The second set of the soil column experiments were carried out using a constant pressure head that was gradually achieved by pouring water through a garden hose water nozzle with a "rainfall-like" showerhead on top of the soil column and maintained using this nozzle with a showerhead. In the conducted experiments air could only escape through the soil column surface. The last set of soil column experiments (three additional experiments) resembled the first five soil column experiments; they were conducted using a constant pressure head that was instantaneously achieved by pouring water on top of the soil column but maintained by pouring water through a garden hose water nozzle with a "rainfall-like" showerhead on top of the soil column like in the second set of the soil column experiments.

2.3.1 First Set of Infiltration Experiments

Each of the first four soil column infiltration experiments followed the same general procedure. First, a fixed large amount of water was poured onto the soil surface of the soil column to simulate a very high intensity rainfall rate. To clarify further, water was carefully poured onto a thin plastic mesh positioned on top of the soil column

surface. This was done to prevent abrupt development of "cracks" and depressions in the top soil layer from pouring large amounts of water on the soil column. Water was continued to be poured onto the soil column until a fixed level of water of 1.5 cm above the soil surface of the soil column was achieved. Second, after ponding and after constant head of 1.5 cm above the soil column was achieved, two pumps were turned on to pump water in order to maintain constant head above the soil column surface and to allow for the continuous simulation of rainfall. Each pump pumped water at the rate of 290 cm d^{-1} (12.07 cm hr^{-1}, 3.35 x 10^{-5} m s^{-1}, or 2.0 mm min^{-1}). Note that a single pump pumping at a rate of 12.07 cm hr^{-1} would not have been adequate to simulate high intensity rainfall rate since a single pump pumping rate is less than the measured saturated hydraulic conductivity, K_{ns} of the tested soil sample. Hence, two pumps were used for the duration of each experiment. If the water above the soil column surface (constant head) fell below 1.5 cm above the soil, water was manually poured on top of the soil. The experiment was continued until the amount of water to be added to the soil column was used up. The amount of water (to be added manually or via pumping water onto the soil column) to be added during each experiment was equivalent to the estimated amount of water to raise the water table by at least 10 cm from the previous initial depth to the water table.

2.3.2 Second Set of Infiltration Experiments

The second set of infiltration experiments consisted of three soil column experiments that were carried out using a constant pressure head that was gradually achieved by applying water through a garden hose water nozzle with a 3"- in diameter

showerhead set on a "shower" pattern. Prior to ponding, simulated rainfall rate of 825 mL/23.9 sec (34.52 mL s^{-1}, 59.46 cm hr^{-1}) was applied over the surface of the soil column using a showerhead. This rate was applied until constant head of 1.5 cm was attained. After that, the rate of simulated rainfall application was gradually decreased or increased to maintain the constant head on top of the soil surface. Note that locking clip and control switch features of the garden hose nozzle allowed continuous water flow as well as allowed to adjust the rate of "rainfall-like" application.

2.3.3 Third Set of Infiltration Experiments

Three other experiments were carried out using a constant pressure head that was achieved by pouring a large amount of water on top of the soil column, like in the first set of infiltration experiments, to achieve instantaneous ponding and H_0. A constant ponded head on top of the soil column surface H_0 was maintained by applying water through a garden hose water nozzle with a "rainfall-like" showerhead. The rate of water application through the shower nozzle was decreased or increased to maintain a constant ponded head H_0.

2.3.4 Data Collection

Changes in soil moisture, pressure readings, water level and barometric pressure readings were recorded for the duration of each experiment and between the experiments to monitor changes. Times were recorded to designate the beginning of the experiment,

the start of pumping or addition of water through the shower nozzle, and the end of the experiment. At the end of each soil experiment the column was covered to eliminate any potential loss of water to evaporation.

2.4 Boundary Conditions

Prior to each set of infiltration experiments, the soil column was air-dried and the water table was drained from the bottom of the soil column to reach initial conditions. The initial conditions for experiment 1 (see Table 1 below) were obtained by draining the soil column to a piezometric level at z = 162 cm below the soil column surface. The initial conditions for experiment 2 consisted of the water table being at z = 128 cm below the soil column surface. The initial conditions for experiments 3 and 4 consisted of the water table being at z=103 cm and z=61 cm respectively. The boundary conditions for the first four experiments consisted of a constant head H_0 = 1.5 cm of water at the soil surface and a zero flux of air and water at the bottom boundary. As previously mentioned, constant head boundary conditions were maintained by pumping water at a constant rate of 290 cm d^{-1} (3.35 x 10-5 m s^{-1} or 2.0 mm min^{-1}).

The initial conditions for experiment 5, 6,7, and 8 consisted of the water table being at z = 127 cm, z = 107 cm, z = 93 cm, and z = 74 cm below the soil column surface respectively. The boundary conditions for these four experiments were a constant head of 1.5 cm of water at the soil surface and a zero flux of air and water at the bottom boundary. As previously mentioned, constant head boundary conditions were maintained by adjusting the rate of simulated rainfall application through a garden hose water nozzle.

The initial conditions for experiment 9, 10, and 11 consisted of the water table being at z = 61 cm, z = 144 cm, and z = 109 cm respectively. The boundary conditions for these experiments were a constant head of 1.5 cm of water at the soil surface and a zero flux of air and water at the bottom boundary. Constant head boundary conditions were maintained by adjusting the rate of simulated rainfall application through a garden hose water nozzle. Table 1 summarizes initial conditions.

Table 1: Initial Depth to the Water Table

Experiment no.	Date	Depth to the water table (cm)	Constant pressure head H_0 (cm)
1	06.23.2009	162	1.5
2	06.30.2009	128	1.5
3	07.14.2009	103	1.5
4	08.22.2009	61	1.5
			1.5
5	06.02.2010	127	1.5
6	06.08.2010	107	1.5
7	06.11.2010	93	1.5
8	06.15.2010	74	1.5
			1.5
9	06.22.2010	61	1.5
10	07.07.2010	144	1.5
11	07.13.2010	109	1.5

CHAPTER 3: MODIFIED GREEN AND AMPT INFILTRATION MODEL

3.1 Methodology Briefing

As described in previous chapters, air compression significantly affects infiltration and cannot be ignored especially when dealing with conditions of intense rain, shallow water table environment, and irrigated fields. Attempts to model air compression and air counterflow in the conditions when air does not escape freely were made by many scientists. Morel-Seytoux and Khanji (1974), Wang et al. (1997), and Hammecker et al. (2003) were able to obtain reasonable results modeling air compression and air counterflow effects. Their proposed infiltration equations are based on the piston-type Green and Ampt (1911) infiltration model that includes an air pressure term. Sabeh (2004) suggested a model similar to the one proposed by Morel-Seytoux (1973). To account for air compression and air counterflow, Sabeh (2004) estimated air pressure at each time step by calculating "air flux out of the soil and applying the perfect gas law for the remaining mass and volume of air ahead of the wetting front." This proposed model combines methodology presented by Morel-Seytoux and Khanji (1974), Wang et al (1997), Hammecker et al. (2003), and Sabeh (2004). Although being very similar to Sabeh's (2004) conceptual model, this model updates air pressure by calculating air flux and the remaining air volume each wetting front increment ΔL. This chapter describes the model.

3.2 Model Assumptions

Since proposed equations were derived on the basis of the Green and Ampt (1911) model, assumptions of the original Green and Ampt (1911) still hold. The assumptions of the proposed model are the following:

- Sharp wetting front. This is not a bad assumption since generally soils with uniform pore shapes, like sand, exhibit a sharp wetting front (Tindall 1999). The model was experimentally tested on the soil column filled with uniform sand;
- Homogeneous soil profile (value of hydraulic conductivity is the same at every point);
- Constant initial soil moisture content;
- The soil is nearly saturated behind the advancing wetting front;
- Constant ponding pressure head;
- Air pressure ahead of the wetting front is constant during each wetting front depth increment;
- Another assumption is that air is confined ahead of the wetting front and could only escape through the soil surface.
- Another assumption of the model is that soil infiltration capacity (infiltration rate at which soil can absorb water once ponding is reached) is attained instantaneously as if a layer of water is applied instantaneously and a constant head is maintained at the soil surface.

- As already stated earlier, an important assumption is that infiltration in the unsaturated or vadose zone is a linear process and natural hydraulic conductivity does not change as water percolates through the soil column (Besbes and de Marsily 1984).

Additional limitations of the introduced model include the following:

- The model is not suited for simulation of movement of the wetting front during non-ponding conditions;
- The proposed model handles simulation of gage air pressure and cumulative infiltration during post-ponding conditions;
- The model does not account for unsteady rainfall;
- Hysteresis is ignored,
- Air entrapment is not accounted for.

3.3 Description of the Proposed Model

It is important to note that the proposed model will only be used for $t>T_p$, since the proposed model does not estimate infiltration while accounting for air compression and air counterflow prior to ponding. In addition, laboratory experiments were designed to test effect of air compression on cumulative infiltration during post-ponding conditions.

The proposed model is represented by the general infiltration equation which is of the type proposed by Morel-Seytoux (1973), Wang et al. (1997), Hammecker et al. (2003), and Sabeh (2004):

$$f = \frac{dF}{dt} = K_{ns} \frac{H_0 + H_c + L - H_a}{L} \qquad \text{Equation 32}$$

where:

- f = infiltration rate [m/hr],
- t = time [hr],
- K_{ns} = hydraulic conductivity at natural saturation [m/hr],
- H_0 = ponded head at the soil surface [m of water],
- H_c = wetting front suction head [m of water] also known as capillary potential,
- L = depth to a sharp wetting front or length of the infiltration zone [m],
- H_a = gage air pressure head just ahead of the advancing wetting front [m].

Equation 29 has a cumulative infiltration depth term. F, which is calculated as following:

$$F = L(\theta_{ns} - \theta_i), \qquad \text{Equation 33}$$

where θ_{ns} [m^3/m^3] is the water content at natural saturation and θ_i [m^3/m^3] is the initial water content.

Two approaches of estimating gage air pressure head H_a were considered: without air counterflow and with air counterflow. Both approaches were compared to the experimental results.

3.3.1 Quantification of Gage Air Pressure without Counterflow

Gage air pressure without counterflow can be modeled using Boyle's law that describes the relationship between the pressure of the trapped gas and its volume (Zumdahl and Zumdahl 2003). Boyle's law can be presented by the following:

$$PV = k \qquad \text{Equation 34}$$

where k is constant. According to Boyle's law the product of volume and pressure is constant for a given sample of air at a specific temperature (Zumdahl and Zumdahl 2003). This means that Boyle's law can be successfully applied to model air pressure without accounting for air counterflow since Boyle's law is applied to the same sample of air without any loss of air mass.

In the absence of counterflow, air pressure continues to build up below the wetting front as air is prevented from exiting the soil; hence, Boyle's law can be applied. If air behaves likes a perfect gas than the absolute air pressure just ahead of the advancing wetting front, H_{abs}, [m of water], is governed by:

$$H_{abs}(D - L) = H_{atm} D\,, \qquad \text{Equation 35}$$

or, after rearranging:

$$H_{abs} = H_{atm}(\frac{D}{D-L}),$$ Equation 36

where H_{atm} is atmospheric pressure [m of water] and D is a depth to an impermeable layer or a water table depth [m]. This equation states that absolute pressure of air is larger than atmospheric, as the vertical domain occupied by air shrinks from D to D-L. The gage air pressure equals to the following:

$$H_a = H_{abs} - H_{atm},$$ Equation 37

and, hence:

$$H_a = H_{atm}\frac{L}{D-L}.$$ Equation 38

where H_{atm} is the atmospheric air pressure (≈ 1032 cm) (Hammecker et al. 2003). For standard atmospheric pressure (≈ 1032 cm), Figure 2 below shows the air pressure head build up as a function of the depth to the water table D, for four wetting front propagation depths L. Figure 2 illustrates that gage air pressure rises with decreasing depth to the water table D and with wetting front propagation depth L. However, from Figure 2 it can be speculated that it is the relationship of the wetting front depth L to the depth to the water table D that drives the gage air pressure up. Notice from Figure 2 how for the wetting front propagation depth L=0.2 m and for the depth to the water table D = 0.25, gage air pressure head is very large (≈ 4 m). Hence, Figure 2 demonstrates that it is important to account for air counterflow. In the study we compare experimental results with modeled results with air counterflow and without air counterflow.

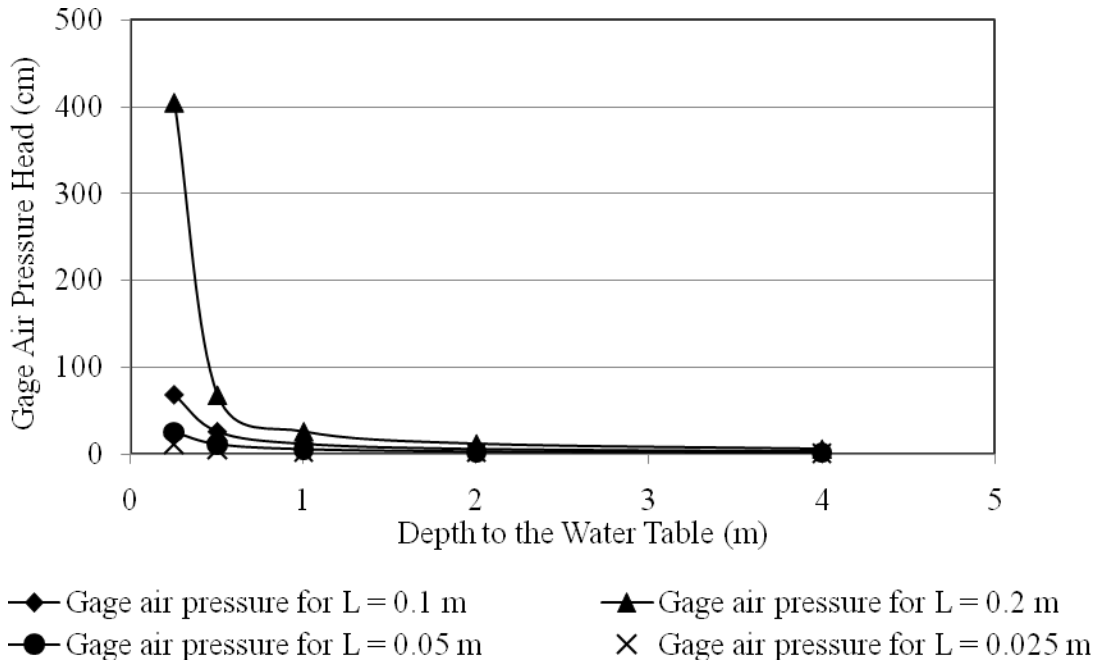

Figure 2: Gage Air Pressure Head for Different Wetting Front Depths

By looking at Equation 32, it is important to note that the air pressure head H_a, in comparison to the terms to the left of H_a in Equation 32, can be large even for a deep water table, which may shut off infiltration. Without counterflow, Equation 32 can overestimate air pressure and create an unrealistic drop in cumulative infiltration (Sabeh 2004). Counterflow of air allows for the release of air pressure as air exits the soil and hence is more applicable in modeling infiltration under intense rainfall conditions, ponding pressure head, and in shallow water table environments.

3.3.2 Quantification of Gage Air Pressure with Counterflow

While water infiltration reduces the available air volume and increases pressure, counterflow releases air mass, reduces the available air volume and reduces gage air pressure. As demonstrated above, Wang et al. (1997) adopted Boyle's law to calculate gage air pressure ahead of the advancing wetting front. Since mass and volume of air and the gage air pressure change continuously with advancement of the wetting front as penetrating water compresses air and is followed by the release of some air, Boyle's law cannot be applied (Sabeh 2004). Instead, the perfect gas law should be adapted when modeling air compression with air counterflow (Sabeh 2004):

$$H_a = \rho_a * R * T \qquad \text{Equation 39}$$

where:

- H_a = absolute air pressure [Pa],
- ρ_a = density of air [kg/m^3],
- R = individual gas constant and equals to 286.9 [J/kg ˚K],
- T = absolute temperature [˚K].

The density of air changes with time due to changes in air mass and air volume below wetting front as the wetting front propagates down the soil column. The air volume after a wetting front propagates distance L into the soil column can be found (Sabeh 2004):

$$V = (D - L) * (\theta_{ns} - \theta_i) \qquad \text{Equation 40}$$

Counterflow is an upward flux of air through the wetting front, hence counterflowing air will be calculated as an air mass flux. The approach, to find counterflowing air as an air mass flux, was described by Charbeneau (2000) and adopted by Sabeh (2004). This approach is presented here.

Darcy's law states (Charbeneau 2000):

$$q = -K(\theta)\frac{\partial h}{\partial z}\,, \qquad \text{Equation 41}$$

where:

$$h = \psi + z\,, \qquad \text{Equation 42}$$

and where:

- θ = soil water or moisture content ,
- K = hydraulic conductivity as a function of the soil water content,
- q = Darcy flux,
- h = hydraulic head,
- ψ=capillary head or suction head
- z= elevation head.

Hydraulic conductivity K and capillary head ψ can be expressed as following (Charbeneau 2000):

$$K = \frac{\rho g k}{\mu}, \qquad \text{Equation 43}$$

and,

$$\psi = \frac{p_c}{\rho g}, \qquad \text{Equation 44}$$

where:

- p_c = capillary pressure defined as the pressure difference between the air and the water (Charbeneau 2000),
- ρ = density ,
- g = gravitational acceleration,
- k = intrinsic permeability of the medium,
- μ=dynamic viscosity of the medium.

Hence, for isotropic and homogeneous medium, Darcy's law can be expressed as:

$$q = -\frac{\rho g k}{\mu}\left(\frac{P_c}{pg} + z\right), \qquad \text{Equation 45}$$

For the purposes of calculating counterflowing air mass flux, the force due to gravity can be ignored since the air density is small; hence, Darcy's law for air can be written as:

$$q = \frac{k k_{ra}}{\mu_a}\frac{\partial P_c}{\partial z}, \qquad \text{Equation 46}$$

Notice that an intrinsic permeability k is multiplied by a relative permeability of air k_{ra} to account for that fact that counterflowing air is flowing between the pores filled with water in the vadose zone (Sabeh 2004). Similarly, μ is replaced with μ_a, which is a viscosity of air.

3.3.3 Air Mass Flux Quantification

For a unit cross-sectional area and one-dimensional vertical flow through wetting front L, the mass flux of air, m_f [kg/s], is:

$$m_f = \rho q = \rho \frac{k\, k_{ra}}{\mu_a} \frac{dP}{dL}. \qquad \text{Equation 47}$$

For isothermal condition, it is customary to express the pressure as $P = \rho P_0/\rho_0$ (Charbeneau 2000), where P_0 [Pa] and ρ_0 [kg/m^3] are reference values for the fluid pressure and density at standard atmospheric condition ($P_0 = P_{atm}$). Thus, Equation 47 can be written as (Sabeh 2004):

$$m_f = P \frac{k\, k_{ra}}{\mu_a} \frac{\rho_0}{P_{atm}} \frac{dP}{dL}, \qquad \text{Equation 48}$$

Variable separation yields:

$$m_f dL = \frac{k\, k_{ra}}{\mu_a} \frac{\rho_0}{P_{atm}} (P dP). \qquad \text{Equation 49}$$

Equation 49 is integrated across the wetting front where the pressure changes from P_w below the front to P_{atm} at the land surface (Sabeh 2004). The air mass flux through the wetting front is:

$$m_f = \frac{k.k_{ra}}{\mu_a}\frac{\rho_0}{P_0}\frac{P_w^{\,2} - P_{atm}^2}{2L} \qquad \text{Equation 50}$$

Relative permeability of air is function of the soil air content (Charbeneau 2000):

$$k_{ra} = (1-\Theta)^2(1-\Theta^{(1+2/\lambda)}), \qquad \text{Equation 51}$$

where λ is the pore size distribution index; and $\Theta = \frac{\theta_{ns} - \theta_r}{n - \theta_r}$ is the normalized water content in the Brooks and Corey (1966) model. The air relative permeability k_{ra} equation (Equation 51) suggests that air flows through the fraction of the pore space between porosity and water content at natural saturation. The wetting front suction head was calculated using Brooks and Corey (1966) model parameters and the equation below (Nachabe and Illangasekare 1994):

$$H_c = \frac{2+3\lambda}{1+3\lambda}h_b, \qquad \text{Equation 52}$$

where $\varepsilon = 3 + 2/\lambda$ and h_b [m] is the Brooks and Corey bubbling pressure.

3.3.4 Gage Air Pressure Quantification

Air pressure was calculated by applying the perfect gas law to remaining air mass occupying the pore space to capture the impact of reduction in air volume on pressure:

$$H_a = \frac{P_w}{\rho_w g} - H_{atm}$$ Equation 53

where H_{atm} is the standard atmospheric pressure head (≈10.32 cm).

3.3.5 Quantification of Cumulative Infiltration

Cumulative infiltration is calculated using:

$$F = L(\vartheta_{ns} - \vartheta_i)$$ Equation 54

where:

- L = wetting front propagation depth,
- θ_{ns} = soil moisture content at natural saturation,
- θ_i=initial soil moisture content.

3.3.6 Ponding Time Quantification

Ponding time is calculated using the following equation (Sabeh 2004):

$$T_p = K_{ns} H_c \frac{\theta_{ns} - \theta_i}{i * (i - K_{ns})}$$ Equation 55

where i is the rainfall rate.

3.3.7 Quantification of Wetting Front Depth at Ponding Time

Wetting front depth at ponding time is calculated using (Sabeh 2004):

$$L_p = \frac{K_{ns} H_c}{i - K_{ns}} \qquad \text{Equation 56}$$

3.3.8 Quantification of Cumulative Infiltration at Ponding Time

$$F_p = K_{ns} H_c \frac{\theta_{ns} - \theta_i}{i - K_{ns}} \qquad \text{Equation 57}$$

3.4 Incorporating Infiltration Model into the Microsoft Excel Spreadsheet

The equations described in the previous sections have been used in the Microsoft Office Excel 2007 to model gage air pressure and cumulative infiltration. In addition to modeling cumulative infiltration while accounting for air compression and air counterflow, the Microsoft Office Excel 2007 was also used to model gage air pressure and cumulative infiltration values of the original Green and Ampt (1911) infiltration equation that did not account for air compression and air counterflow. The following section describes the steps used to incorporate the proposed Green and Ampt based infiltration model in to the Microsoft Office Excel 2007:

- The first step in the program is to input all the initial values and modeling parameters, including:

- i= rainfall intensity (cm/hr) ,
- D = depth to water table (m),
- θ_i = initial water content (%),
- n = porosity (%),
- θ_{ns} = saturated water content (%),
- θ_r = residual water content (%); Brooks and Corey (1966) model parameter,
- K_{ns} = hydraulic conductivity at natural saturation (cm/hr),
- λ = pore size distribution index; Brooks and Corey (1966) model parameter,
- h_b = bubbling pressure head (m); Brooks and Corey (1966) model parameter,
- K_s = saturated hydraulic conductivity,
- H_0 = ponding depth at the surface of the soil column (m).

- Model calculates wetting front suction head H_c; ponding time T_p (min); cumulative infiltration up to ponding time F_p (m); and a wetting front propagation depth L_p (m). All these parameters are used in post ponding modeling of gage air pressure head H_a and cumulative infiltration F.

- Air density is calculated using $\rho_a = \frac{P_{atm}}{RT}$.

- Choose a small increment in wetting depth ΔL and calculate initial air volume $V = (D-L_p) * (\theta_{ns} - \theta_i)$ where L_p is the wetting front propagation depth at ponding time T_p.

- Once initial air density and air volume are known initial air mass is calculated $m_a = \rho_a * V$.

- Next, air mass flux is calculated using $m_f = P \frac{k\, k_{ra}}{\mu_a} \frac{\rho_0}{P_{atm}} \frac{dP}{dL}$.

- For simplicity of calculations absolute pressure (water plus air pressure) at the wetting front depth L_p at time to ponding T_p is assumed to equal to standard atmospheric pressure (=101000 Pa). The assumption was tested and results showed that choice of the initial absolute pressure at the wetting front does not have an impact on consecutive calculations of gage air pressure and cumulative infiltration. This is given that the wetting front propagation depth L_p at ponding constitutes 10% or less of the depth to the water table D.

- Initial gage air pressure head at the wetting front is calculated. At T_p, it is equal to 10.32 cm of water.

- Time increment Δt is calculated using $\Delta t = \frac{L\Delta L(\vartheta_{ns} - \vartheta_i)}{K_{ns}(H_0 + H_c + L + H_a)}$. This was derived from knowing that $\Delta t = \frac{\Delta F}{f}$, $f = K_s \frac{H_0 + H_c + L - H_a}{L}$, and $\Delta F = \Delta L(\vartheta_{ns} - \vartheta_i)$.

- Initial total time is equal to T_p since gage air pressure values and cumulative infiltration are modeled during post ponding. Total time is calculated $T = T_p + \Delta t$.

- Cumulative infiltration F is calculated using $F = (\vartheta_{ns} - \vartheta_i)L$. At this point initial series of calculations is complete. Next series of calculations is presented next. It is repeated throughout the modeling process with air mass flux and air mass being updated during post ponding cumulative infiltration calculations.

- Wetting front propagation depth is calculated using $L_2 = L_p + \Delta L$. Consecutive wetting front propagation depth is calculated using $L_3 = L_2 + \Delta L$.

- Next air volume is calculated using $V = (D - L_2) * (\theta_{ns} - \theta_i)$.

- Air mass below the wetting front is updated using $m_2 = m - m_f$.

- Next air density is calculated using updated air mass and air volume.

- Absolute pressure below the wetting front is calculated using ideal gas law $P_w = \frac{P_{atm}\rho}{\rho_0}$ and gage air pressure head is calculated $H_a = \frac{P_w}{\rho_w g} - H_{atm}$.

CHAPTER 4: RESULTS AND DISCUSSION

4.1 Introduction

This chapter presents experimental validation of the modified Green and Ampt model accounting for air compression and air counterflow using the proposed algorithm created in the Microsoft Office Excel 2007. The first section contains representative results of laboratory experiments conducted in the soil column. The second section presents a comparison between the observed experimental results and the results modeled using the proposed algorithm of the infiltration model. In this section observed and modeled values of gage air pressure and cumulative infiltration are compared. The third section compares the results of the original Green and Ampt (1911) infiltration model and the proposed Green and Ampt infiltration model accounting for air compression and air counterflow.

4.2 Experimental Results

Laboratory experiments using a transparent soil column (45.7 cm i.d. and 180.34 cm sol column height) were conducted to test the results of the proposed Excel algorithm of the infiltration model that accounts for air compression and air counterflow. Detailed

description of the experimental setup and conducted soil column experiments are presented in CHAPTER 2.

To analyze results from the laboratory column studies, moisture characteristics curves for wetting conditions were developed. Hysteresis was ignored to simplify the analysis. The power law model of Brooks and Corey (1966) was used to estimate the soil characteristics curve parameters (Charbeneau 2000). Analysis of a number of observed soil moisture characteristic curves and application of the Brooks and Corey (1966) model indicated that bubbling or air entry capillary pressure head equals h_b= 26 cm and the pore size distribution index λ= 1.53. The total porosity of the sand was found to be n=0.37 cm^3/cm^3 and the irreducible water content was taken as θ_r= 0.045 cm^3/cm^3.Using the Brooks and Corey (1966) model, the largest water content expected in the soil column profile , also known as water content at natural saturation, was found to be θ_{ns} = 0.30 cm^3/cm^3. As mentioned earlier a number of constant head permeability tests indicated an average water conductivity K_s of 322 cm d^{-1} (13.42 cm hr^{-1}, 3.73 x 10-5 m s^{-1} , or 2.2 mm min^{-1}) without air effects. However, in algorithm simulations a saturated hydraulic conductivity K_s = 20 cm hr^{-1} was used since this value produced a better fit. Other parameters were used as mentioned.

4.2.1 Observed Gage Air Pressure

Changes in pressure were measured every two minutes and every minute at the pressure transducers located every 10 cm below the soil surface in the first and second set of experiments respectively (see CHAPTER 2). The objective was to examine air

pressures below the wetting front. Another objective was to determine whether the depth to the water table, rainfall intensity, rainfall application, and any of the water characteristics curve initial conditions affected gage air pressure. It is important to note that to validate the proposed infiltration model, the focus was on the air pressure changes only during the experiment, in other words during the application of water on top of the soil column and until the application of water stopped.

Unfortunately the equipment to measure dynamic changes in air pressure below the wetting front, as water infiltrated in, was not available and only overall pressure (water + air) at the pressure transducers was measured. However to estimate gage air pressure ahead of the wetting front, data recorded by well data loggers and data from pressure transducers located just above and below the water table, was used. In most of the experiments, throughout the duration (during application of water and right after water application was stopped) the wetting front never reached the water table. Hence, it is believed that pressure transducers, located at the water table, recorded gage air pressure. Gage air pressure values obtained from pressure transducers were compared to gage air pressure values obtained using well data loggers. Gage air pressure values from well data loggers and pressure transducers were found to be comparable (see Figure 3).

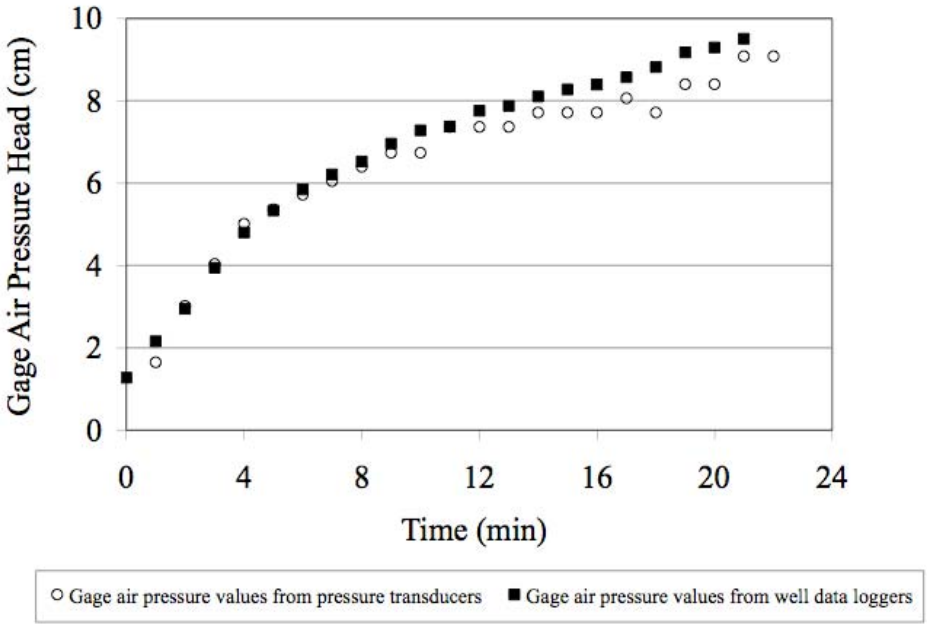

Figure 3: Comparison of Gage Air Pressure Values Obtained from Pressure Transducers and from Data Loggers

As described in CHAPTER 2, laboratory experiments in the transparent soil column were carried out for air confining conditions. Hence, air was trapped ahead of the wetting front and could only escape through the upper layers of the soil column and the soil surface. Gage air pressure ahead of the advancing wetting front was captured by well data loggers that recorded an apparent rise in the water table without elevated moisture content reaching the water table. This occurred during wetting of the soil column. Total number of 11 soil column experiments was conducted to assess air effects on infiltration into the soil column. Table 2 summarizes maximum gage air pressure heads attained during these experiments.

Table 2: Maximum Gage Air Pressure Heads Attained

Experiment	Depth to the water table (cm)	Initial water content (cm^3/cm^3)	Maximum gage air pressure attained (cm)	Cumulative infiltration (cm)
06.23.2009	162	0.0614	10.63	7.67
06.30.2009	128	0.0774	10.02	8.62
07.14.2009	103	0.1203	0.70	8.50
08.22.2009	61	0.244	7.50	1.27
06.02.2010	127	0.0756	7.01	4.15
06.08.2010	107	0.1023	3.33	3.64
06.11.2010	93	0.1472	3.37	2.30
06.15.2010	74	0.2033	3.70	0.24
06.22.2010	61	0.2573	49.40	1.05
07.07.2010	144	0.0683	8.02	6.70
07.13.2010	109	0.0987	15.05	7.06

The Lisse effect was observed during the experimental soil column studies and is shown in Figure 4. Figure 4 shows apparent rise in the water table captured during the soil column experiment performed on 06.30.2009. As shown in Figure 4 water table rose from 127.58 cm (measured from the top of the coil column) to 114.60 cm in 27 minutes (from t = 9:46 am to t = 10:13 am). This is the result of air compression since no change in soil moisture sensors is observed. Notice how sensors 10 and 12 located 98.5 cm and 118.5 cm respectively (measured from the top of the coil column) have not reacted to the addition of water. Table 3 summarizes apparent rises in the water table (the Lisse effect) captured by well data loggers during the soil column experiments. Apparent rise in the water table was captured by well data loggers in all of the soil column experiments

except for the experiments performed on 07.14.09, 08.22.09, 06.11.10, 06.15.10, 06.22.10. This could be attributed to a shallower water table and higher initial soil moisture content.

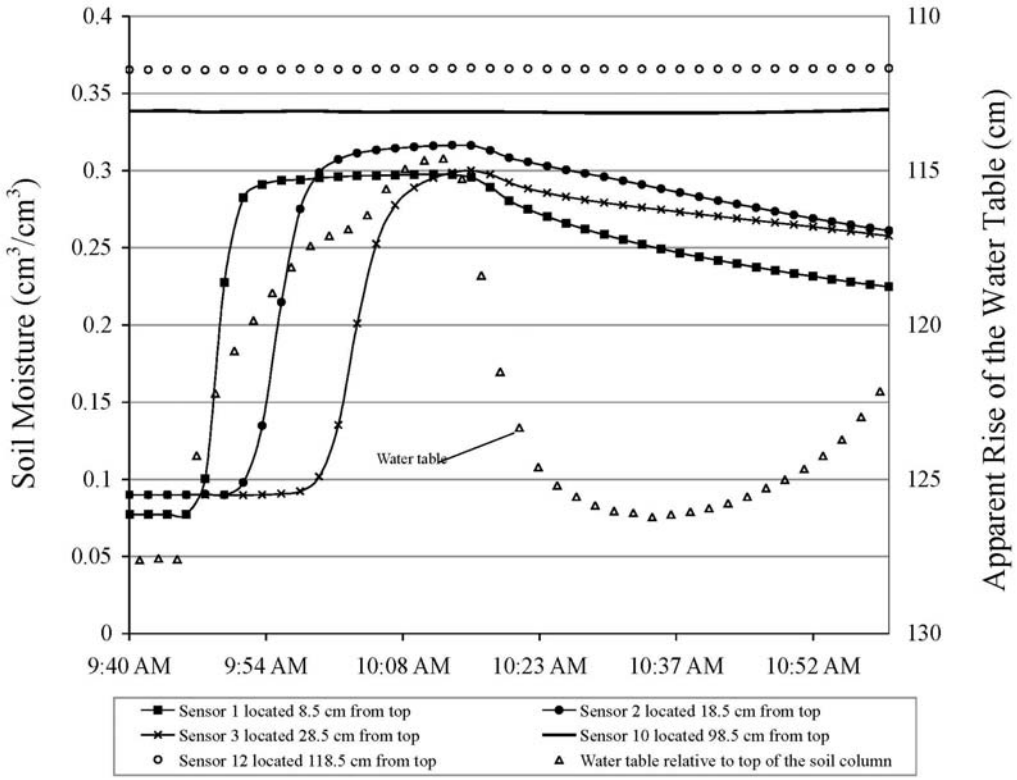

Figure 4: Apparent Rise of the Water Table during Experiment Performed on 06.30.09

Table 3: Highest Observed Apparent Rise in the Water Table

Experiment no.	Date	Duration of the experiment (min)	Time of the highest observed apparent rise in the water table (min)	Apparent rise in the water table (cm)
1	06.23.2009	20	20	8.89
2	06.30.2009	26	26	9.62
3	07.14.2009	30	N/A	N/A
4	08.22.2009	4	N/A	N/A
5	06.02.2010	10	12	6.38
6	06.08.2010	8	N/A	N/A
7	06.11.2010	5	8	2.96
8	06.15.2010	4	N/A	N/A
9	06.22.2010	22	N/A	N/A
10	07.07.2010	14	16	8.2
11	07.13.2010	21	30	10.5

The air pressure recorded ahead of the wetting front was found to increase with time during wetting of the soil column (see Figures below).

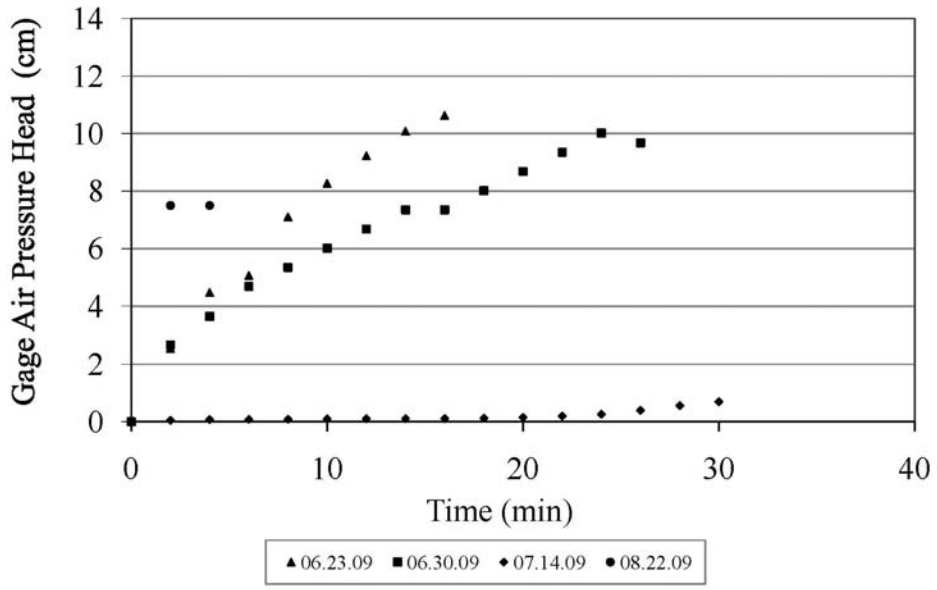

Figure 5: Gage Air Pressure Observed during the First Set of Experiments

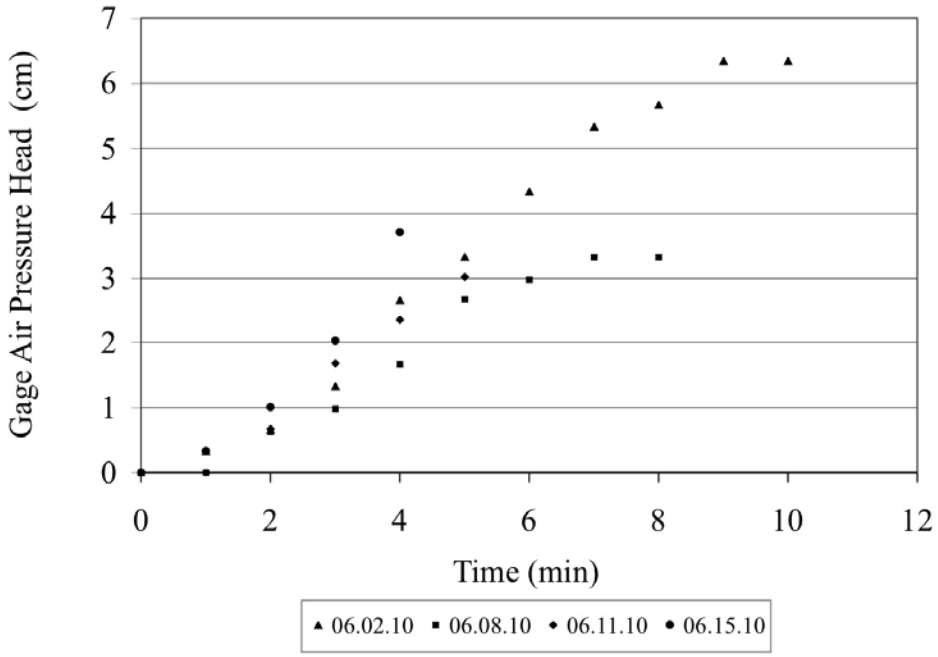

Figure 6: Gage Air Pressure Observed during the Second Set of Experiments

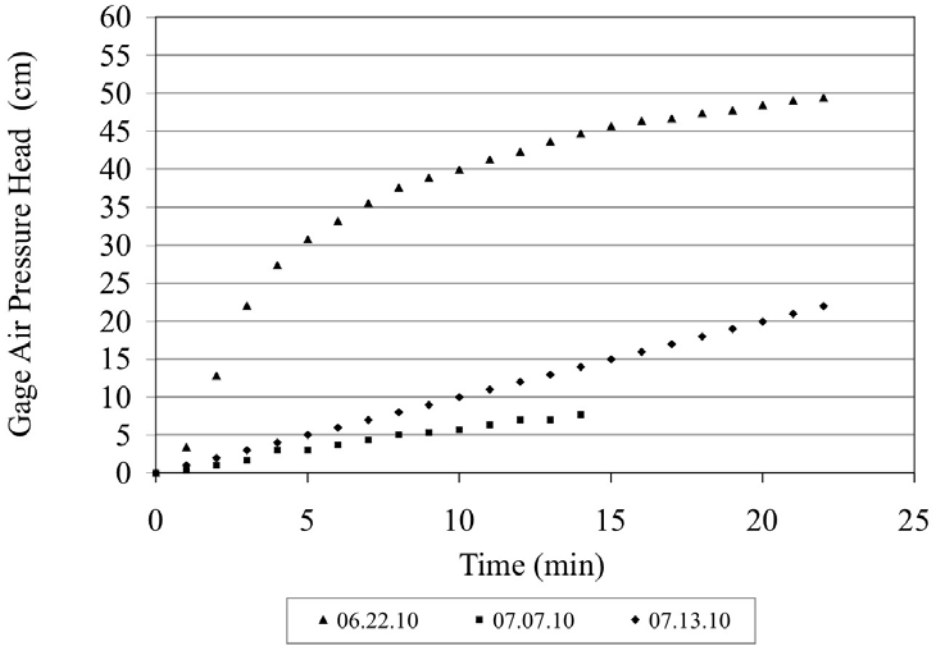

Figure 7: Gage Air Pressure Observed during the Third Set of Experiments

Notice the rise of H_a (≈ 50 cm) during the experiment 9 performed on 06.22.10. This was expected since the experiment started with nearly saturated conditions of the soil column (θ_i = 0.26 cm^3/cm^3) and the depth to the water table D = 0.61 m (see Figure 7).

The experimental results under constant head and air confining conditions showed significant increases in air pressure H_a with time with decreasing depth to the water table and increasing initial moisture content. The maximum pressure H_a attained under a constant ponded head was ≈ 50 cm of water.

As mentioned earlier, in the second series of the soil column experiments, ponding and a constant head of 1.5 cm were gradually attained by applying water. Constant ponded head H_0 was maintained by increasing or decreasing rate of water application. This allowed for a release of air through the soil column surface. In

comparison to the first set of soil column studies smaller gage air pressure values ahead of the wetting front were observed during the second set of experiments.

During experiment 5 performed on 06.02.10 (see Figure 8 below) air pressure rose uniformly to ~6 cm at t~11 min shortly after the application of water stopped. At about t~5 min air bubbles started to erupt from the top of the soil surface. This was not accompanied by decrease in air pressure as initially expected and suggested by Wang et al. (1998). Air eruption stopped at about t~12 min and air bubbles on top of the soil surface were no longer observed since almost all of the water infiltrated in at that time. In general air pressure was found to increase with time during the application of water and decreased shortly after all of the water infiltrated (Figure 5).

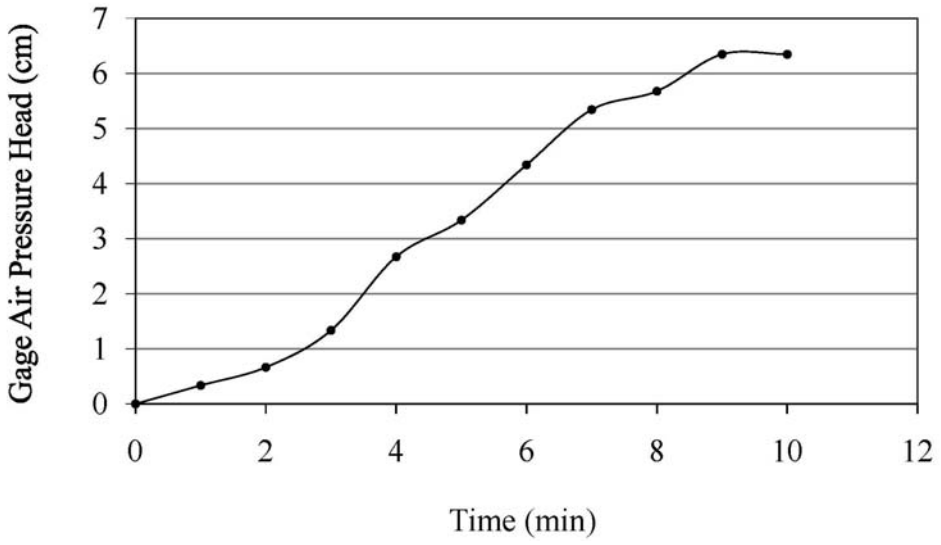

Figure 8: Gage Air Pressure Head Variation with Time during Experiment No.5

Another important observation from the second series of infiltration experiments was that gage air pressure readings recorded were smaller than gage air pressure values recorded during the first series of soil column experiments. Hence, it can be concluded that that the amount of compressed air and hence gage air pressure head readings can depend not only on the initial water content and the depth to the water table but also on the rainfall intensity. Higher gage air pressure readings were observed during the first series of experiments because a constant ponded head was rapidly achieved by pouring a large amount of water. This trapped air in the vadose zone and compressed air ahead of the wetting front causing a rise in the gage air pressure. In the second series of experiments, ponding and a constant ponded head of 1.5 cm were gradually achieved. This allowed air to escape through the upper layers of the soil profile (see Figure 6).

Gage air pressure values from the third set of soil column experiments are shown in Figure 7.

As mentioned earlier, results from the soil column experiments that created a rapid ponded head on top of the soil column showed higher air compression values than soil column experiments that gradually achieved ponding and a constant head on top of the soil column.

It was found that with each subsequent soil column experiment, as the water table got shallower and the initial water content increased, gage air pressure head values recorded by pressure transducers decreased. Soil column experiments with initial depth to the water table $D \leq 1$ m showed no Lisse effect captured by well data loggers. The well, where the data logger was placed, was screened at the bottom of the soil column. If the

well was screened all the way through the soil column the Lisse effect could have been observed. In addition, in deep water table conditions ($D \geq 1$ m), during wetting of the soil column, there is a possibility of a large amount of air being compressed between the advancing wetting front and the impermeable layer such as the water table. The compressed air is pushing on the water table and the well data logger is recording the "apparent" rise in the water table. In shallower water table conditions less air is pushing on the water table and the "apparent" rise is not recorded by well data loggers.

4.2.2 Observed Infiltration Rates

Infiltration rates were also measured during each soil column experiment. Decrease in infiltration rates with each subsequent experiment was observed.

Plots of observed infiltration rates are given in Figures 9, 10, and 11 below. Initial conditions, depth to the water table, initial soil moisture contents, total amount of water added, the highest gage air pressure head attained, as well as the highest infiltration rate attained during each experiment are tabulated in Table 4 below.

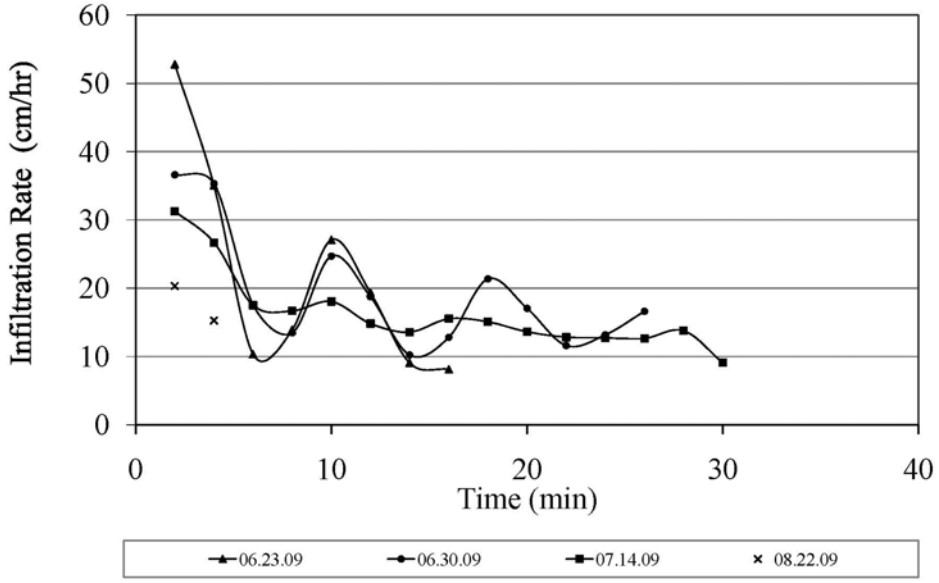

Figure 9: Infiltration Rates Observed during the First Set of Experiments

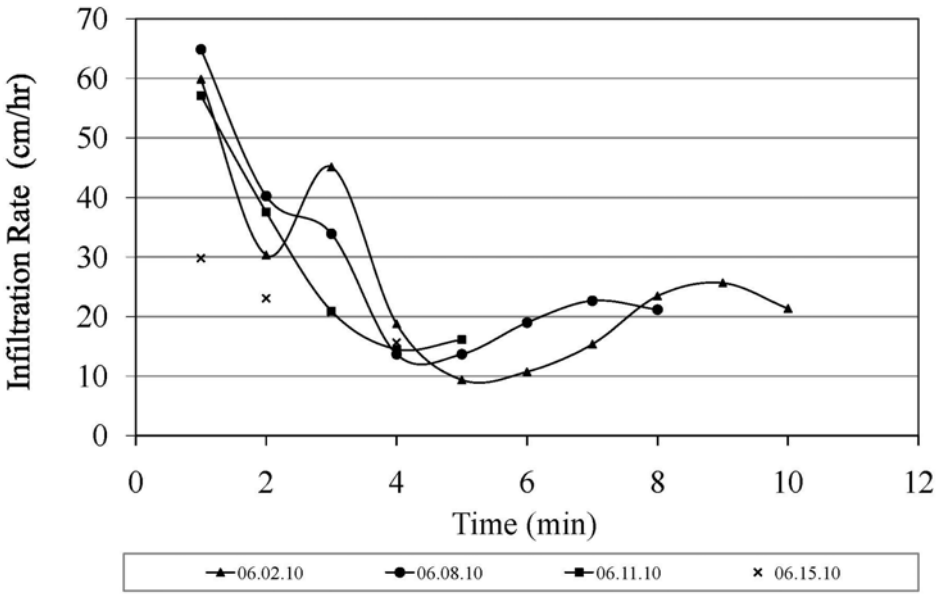

Figure 10: Infiltration Rates Observed during the Second Set of Experiments

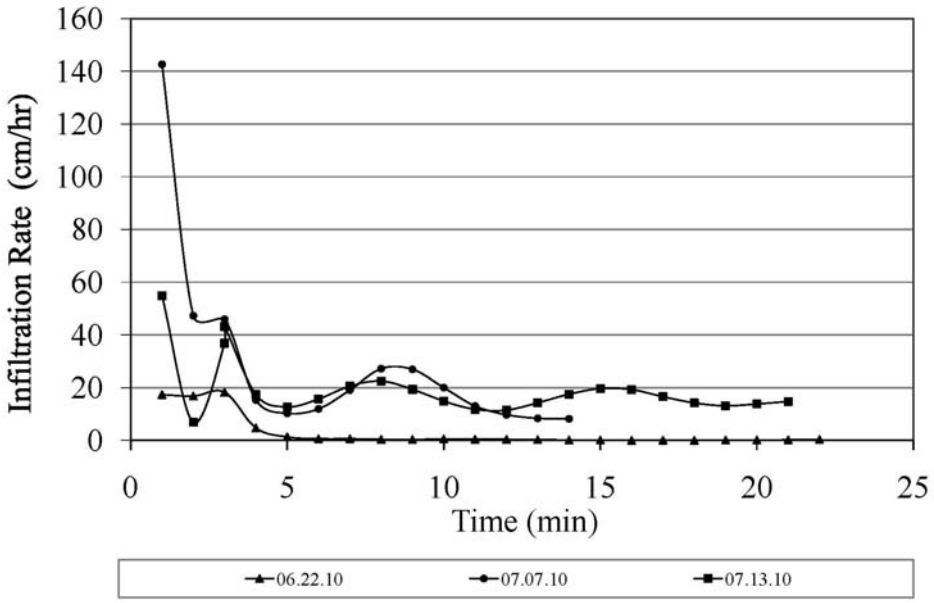

Figure 11: Infiltration Rates Observed during the Third Set of Experiments

Table 4: Maximum Infiltration Rate Attained

Experiment no.	Date	Depth to the water table (cm)	Initial water content (cm^3/cm^3)	Maximum gage air pressure attained (cm)	Highest Inifiltration Rate Observed
1	06.23.2009	162	0.0614	10.63	52.78
2	06.30.2009	128	0.0774	10.02	36.61
3	07.14.2009	103	0.1203	0.70	31.26
4	08.22.2009	61	0.244	7.50	20.32
5	06.02.2010	127	0.0756	7.01	59.82
6	06.08.2010	107	0.1023	3.33	64.85
7	06.11.2010	93	0.1472	3.37	57.07
8	06.15.2010	74	0.2033	3.70	29.82
9	06.22.2010	61	0.2573	49.40	18.23
10	07.07.2010	144	0.0683	8.02	142.65
11	07.13.2010	109	0.0987	15.05	54.87

Figures 9,10,11, and Table 4 show that, for the exception of the experiment performed on 06.22.10, the highest infiltration rate was the first recorded infiltration rate and hence could be assumed to be the "rainfall rate" applied (the rate of addition of water) prior to ponding conditions. The highest infiltration rate during the experiment performed on 06.22.10 was recorded 3 minutes after the start of the experiment. For the exception of the experiments 4,8, and 9, Figures 9,10,11 show oscillations in infiltration rates. Interestingly, the experiments that do not show oscillations in infiltration rates (experiments 4,8,9) are the experiments with the smallest initial depth to the water table and the highest initial soil water content of the series of infiltration soil column studies (see Table 4). However, the reason why the experiments 4 and 8 did not show oscillations was because of the short duration of these soil column experiments, less than 4 minutes.

No oscillations and a nearly constant infiltration rate of the experiment 9 can be attributed to nearly saturated conditions of the soil column and the small depth to the water table. In addition, this could have occurred if the counterflowing air never escaped the soil surface during the addition of water. In addition, during the experiment 9, the highest gage air pressure head value was nearly 50 cm.

Plots of infiltration rate, cumulative infiltration and gage air pressure as functions of time for all soil column experiments are presented in Appendix B. During all of the soil column experiments increases in infiltration rate associated with decreases in gage air pressure were not observed. Instead oscillatory behavior of infiltration rates and a gradual increase in gage air pressure with time was observed. A counterflowing air breaking through the soil column surface could have caused oscillations in infiltration rates; however, gradually rising gage air pressure did not show signs of air breaking through the soil column surface. It is possible that oscillations in gage air pressure might not have been captured due to the fact that most of the soil column experiments were no longer than 10 minutes. In the literature, the oscillations in gage air pressure were observed when experiments were conducted for 2 hours or longer, although oscillations in gage air pressure due to air breaking through the soil column surface occurred during the first 20 minutes of the experiments (Grismer et al. 1994). Hence, it would not be right to completely discard that infiltration rate oscillations can be caused by a soil air breaking through the soil surface.

Generally, a decrease in infiltration rates with each subsequent experiment was observed. As mentioned before, a decrease in infiltration rates can be attributed to the rise of the water table between the experiments and the reduced soil water storage capacity. It

is important to note that observations during the experiments showed that air began to escape (also known as "bubbling") – through the soil surface – very soon, during the first minute of each conducted soil column experiment. It can be suggested, that the escape of air through the upper soil surface layers is captured in Figures 9,10, and 11 that show infiltration rate oscillations. Notice an abrupt fall in infiltration rates that is generally followed by a spike associated with air having escaped through the soil surface as a counterflow.

4.2.3 Observed Cumulative Infiltration

Cumulative infiltration was directly obtained by measuring changes in soil moisture sensors for the duration of each experiment. From soil moisture sensors' readings, infiltration depth was calculated by numerically integrating the water content profile during a simulated rainfall event. Mathematically, the infiltration rate *f*, with time during a storm is:

$$f_t = \frac{1}{\Delta t} \sum_{i=1}^{n} \left[\left(\theta_i^t - \theta_i^{t-\Delta t} \right) + \left(\theta_{i+1}^t - \theta_{i+1}^{t-\Delta t} \right) \right] \Delta z_i / 2 , \qquad \text{Equation 58}$$

where:

- θ_i^t = volumetric water content at time *t* and sensor *i*,
- $\theta_{i+1}{}^t$ = volumetric water content at sensor *i+1* and time *t*,
- Δz_i = elevation distance between the moisture sensors *i* and *i+1*,

- Δt = two minutes (first set of experiments) and one minute (second and third set) time intervals between measurements.

Infiltration rates were accumulated over time to calculate observed cumulative infiltration depths. Plots of cumulative infiltration as a function of time are given in Figures 12, 13, and 14.

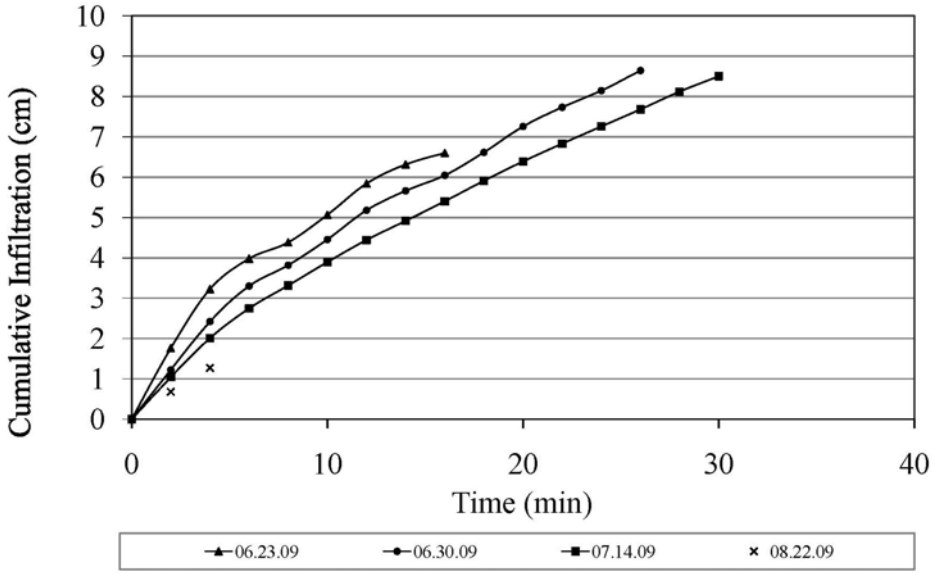

Figure 12: Cumulative Infiltration Observed during the First Set of Experiments

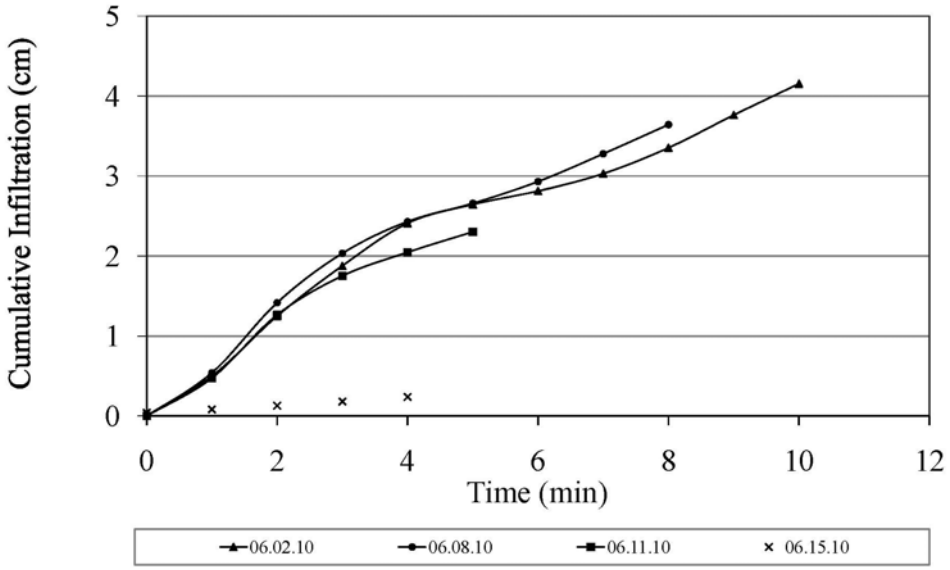

Figure 13: Cumulative Infiltration Observed during the Second Set of Experiments

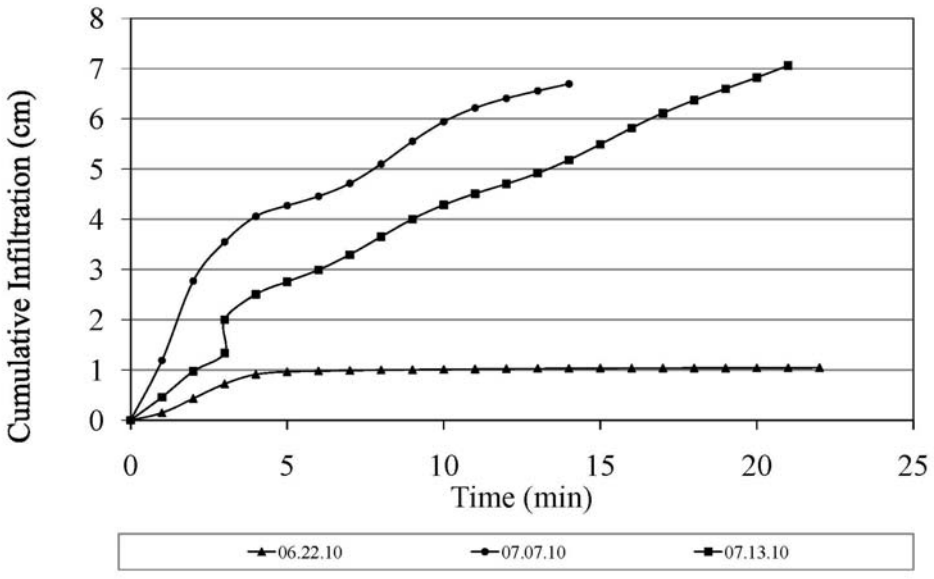

Figure 14: Cumulative Infiltration Observed during the Third Set of Experiments

Figures 12, 13, and 14 show cumulative infiltration for the conducted soil column experiments. Cumulative infiltration curves exhibit similar behavior (slope of the line and oscillations). It can be noted that cumulative infiltration at a particular time t, for instance at t = 6 min, is smaller with each subsequent experiment. For instance, as Figure 12 shows, at t =6 min, during the experiment 1 cumulative infiltration F = 3.98 cm, during the experiment 2, F = 3.30 cm, and during the experiment 3, F = 2.75 cm. This was expected due to the water table rise and the reduced available soil storage with each subsequent experiment.

As previous infiltration studies and this soil column study show there is a relationship between the depth to the water table, storage capacity of the soil profile, cumulative infiltration, and infiltration rates. Conducted experiments suggest that a shallower water table environment means less soil water storage capacity and less cumulative infiltration.

4.3 Comparison of Experimental Results with Modeled Results

This section compares experimental results from the soil column studies with modeled results of gage air pressure and cumulative infiltration values. In the Excel algorithm simulations of modeled values of gage air pressure and cumulative infiltration, air and water physical properties at 20° C were used. Air and water physical properties at 20° C are given in Table 6 (see Appendix A). Besides the physical air and water properties the following parameters were used:

- Brooks and Corey bubbling pressure h_b = 26 cm,

- Brooks and Corey pore size distribution index $\lambda = 1.53$,
- porosity $n = 0.37$ cm^3/cm^3,
- irreducible water content $\theta_r = 0.045$ cm^3/cm^3,
- water content at natural saturation $\theta_{ns} = 0.30$ cm^3/cm^3,
- saturated hydraulic conductivity $K_s = 20$ cm hr-1.

Plots of gage air pressure head values and cumulative infiltration values from the soil column experiments are given in Figures 15 through 32 below. Gage air pressure head values or cumulative infiltration values from the experiments 4 and 9 were not modeled due to the short duration of these soil column experiments.

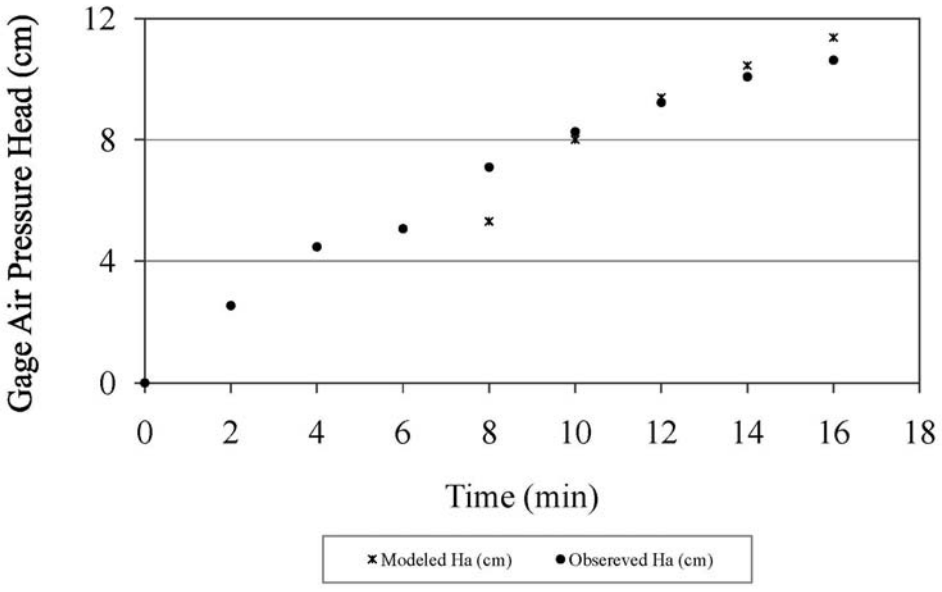

Figure 15: Experiment No. 1 Modeled and Observed Gage Air Pressure Head

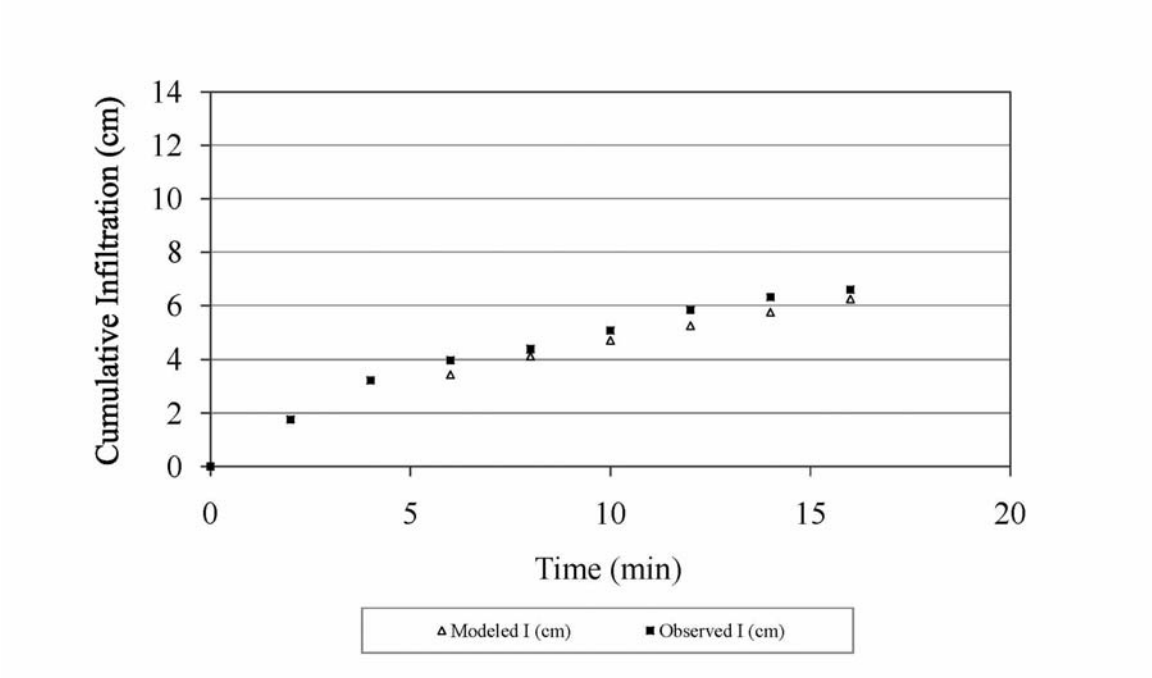

Figure 16: Experiment No. 1 Modeled and Observed Cumulative Infiltration

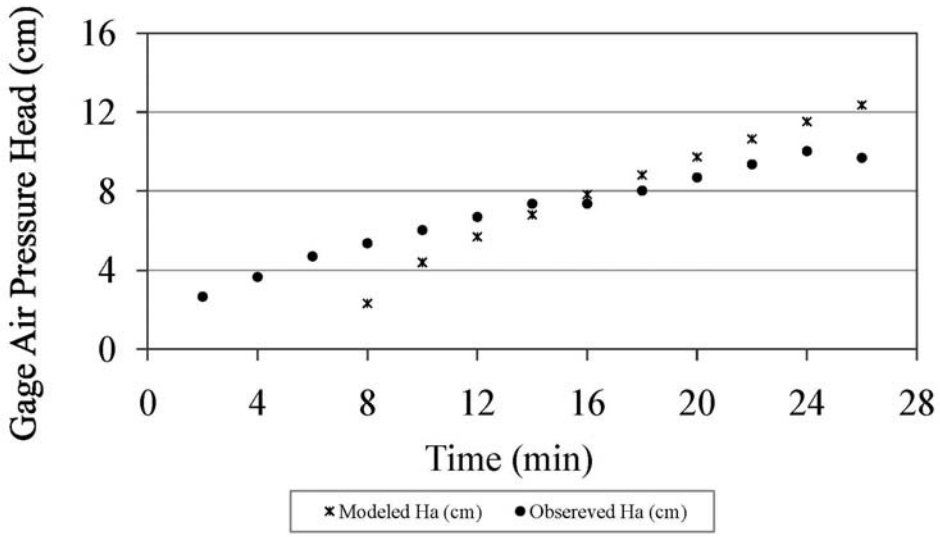

Figure 17: Experiment No. 2 Modeled and Observed Gage Air Pressure Head

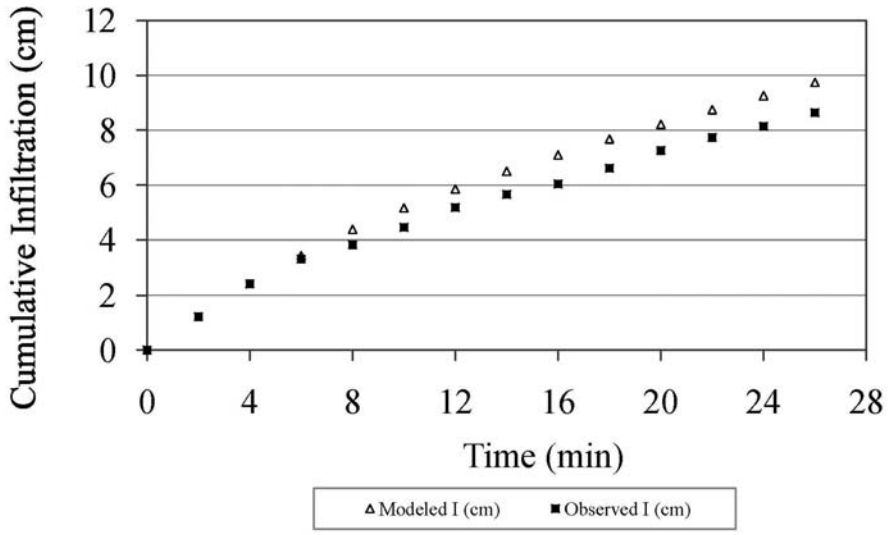

Figure 18: Experiment No. 2 Modeled and Observed Cumulative Infiltration

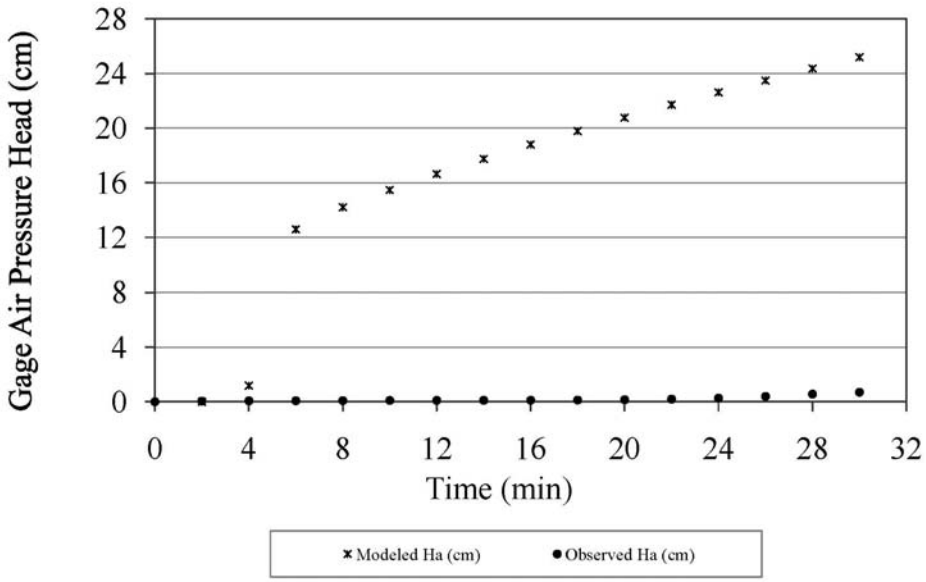

Figure 19: Experiment No. 3 Modeled and Observed Gage Air Pressure

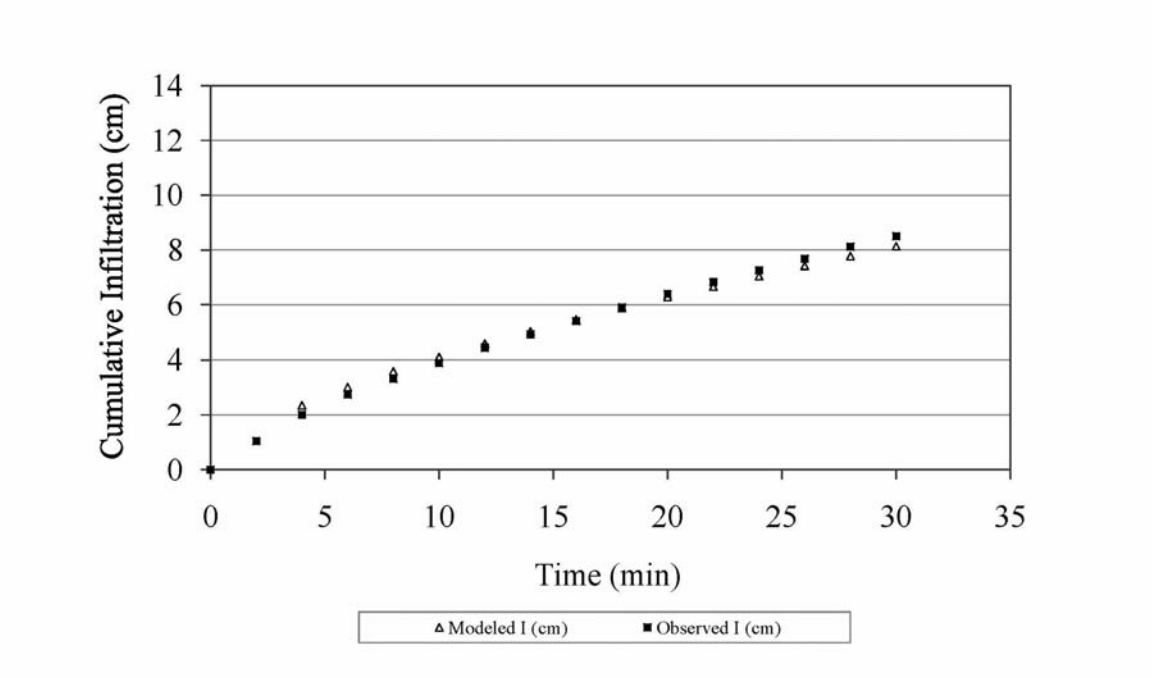

Figure 20: Experiment No. 3 Modeled and Observed Cumulative Infiltration

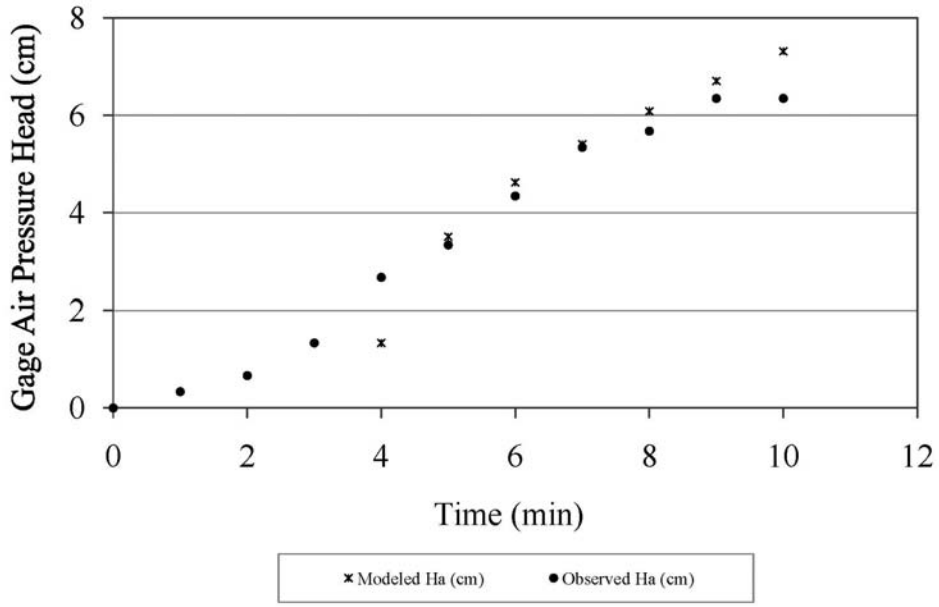

Figure 21: Experiment No. 5 Modeled and Observed Gage Air Pressure Head

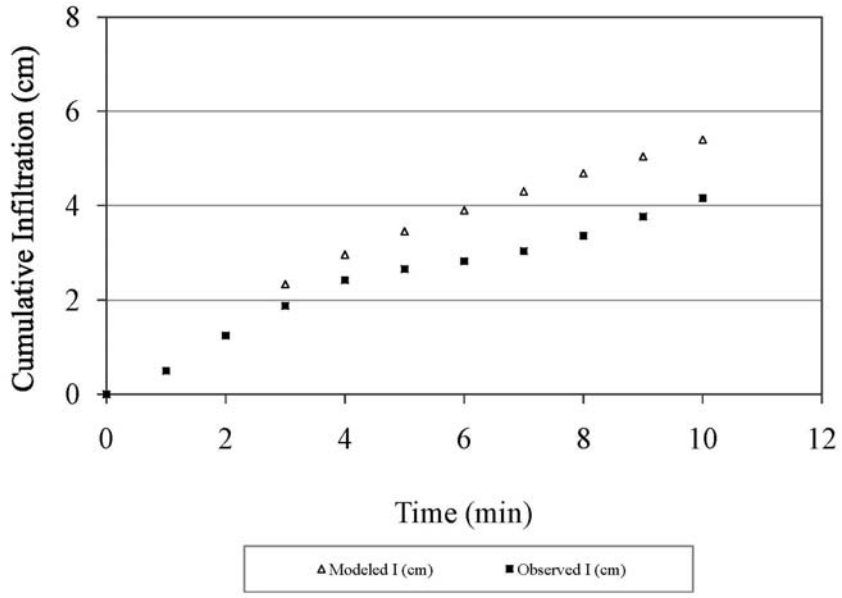

Figure 22: Experiment No. 5 Modeled and Observed Cumulative Infiltration

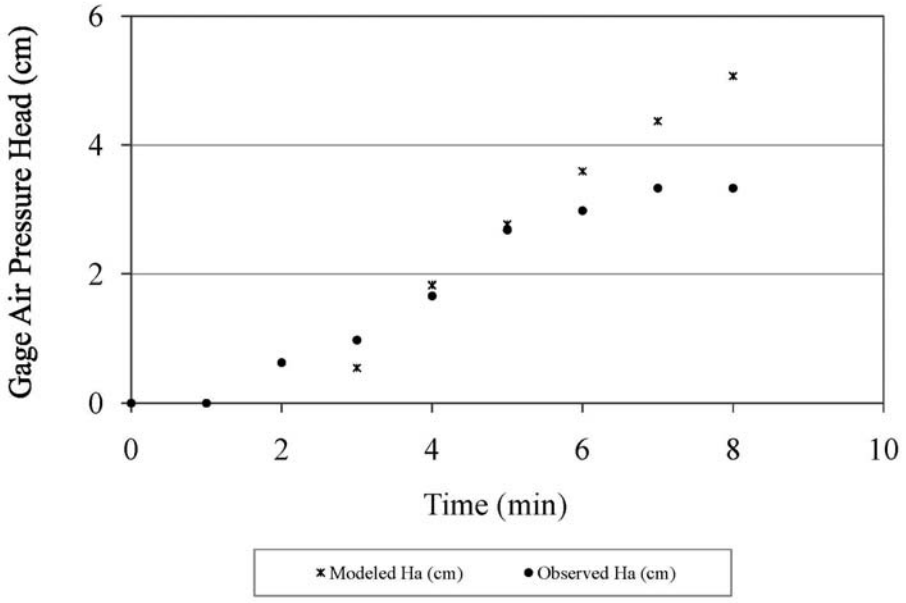

Figure 23: Experiment No. 6 Modeled and Observed Gage Air Pressure Head

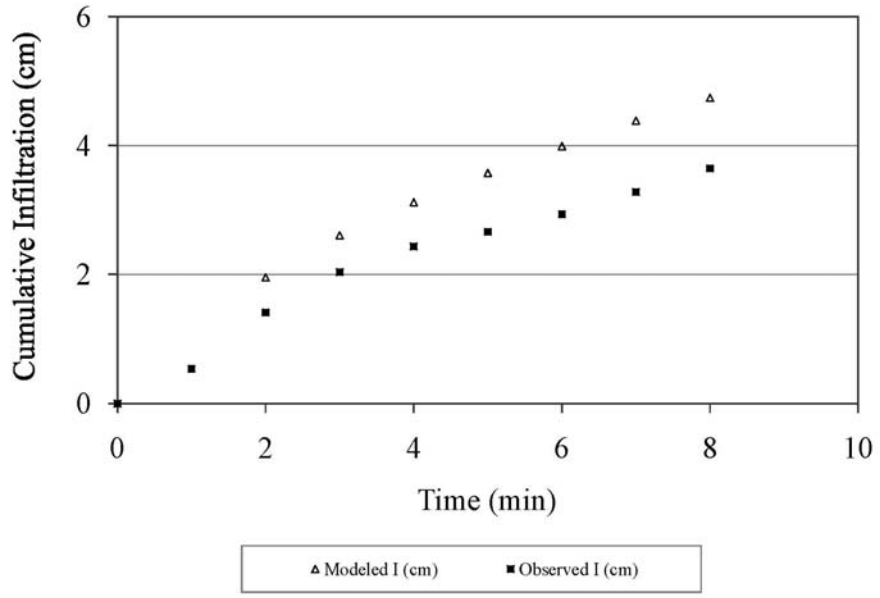

Figure 24: Experiment No. 6 Modeled and Observed Cumulative Infiltration

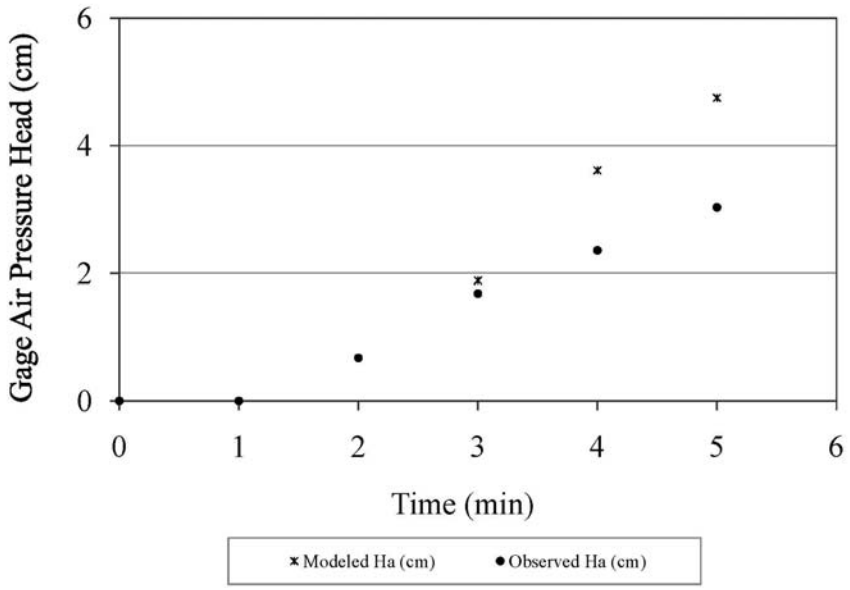

Figure 25: Experiment No. 7 Modeled and Observed Gage Air Pressure Head

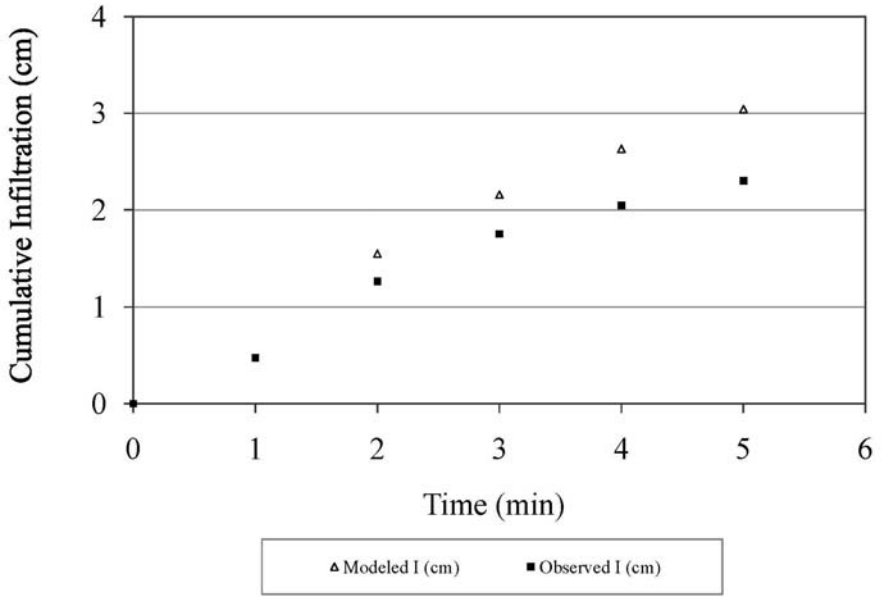

Figure 26: Experiment No. 7 Modeled and Observed Cumulative Infiltration

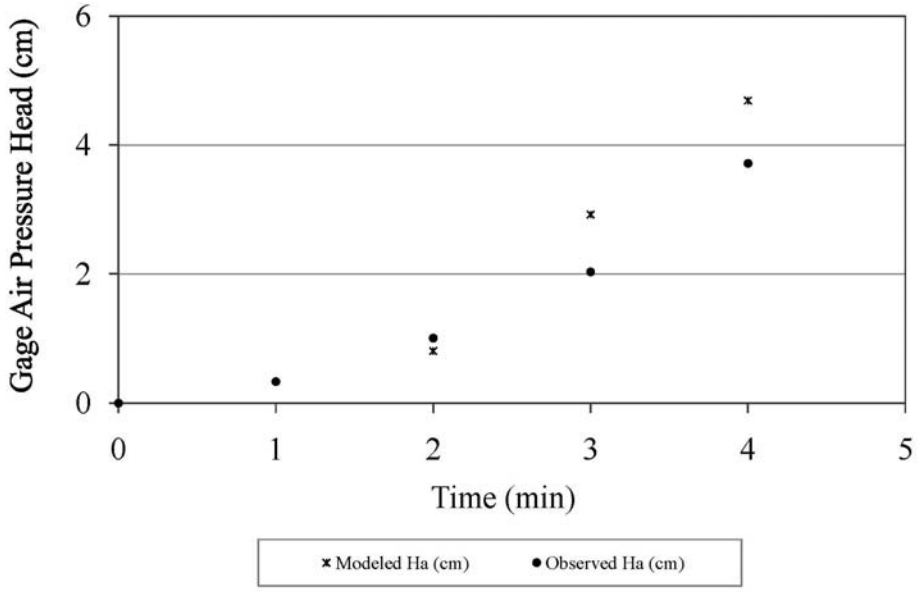

Figure 27: Experiment No. 8 Modeled and Observed Gage Air Pressure Head

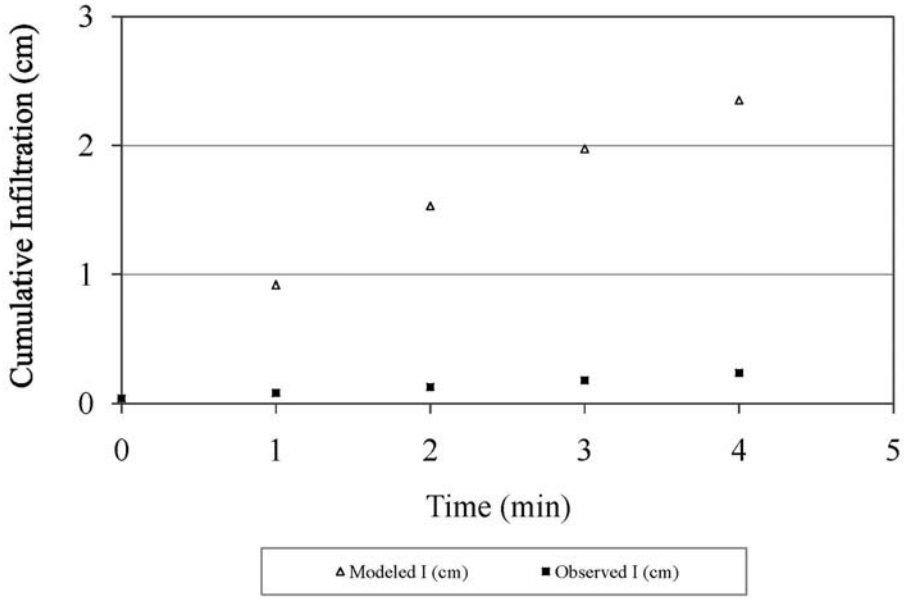

Figure 28: Experiment No. 8 Modeled and Observed Cumulative Infiltration

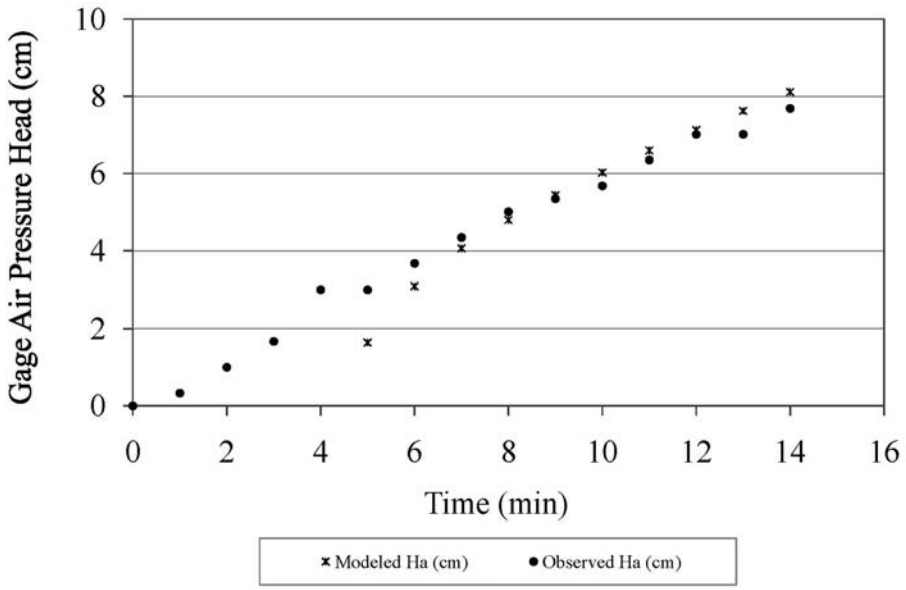

Figure 29: Experiment No. 10 Modeled and Observed Gage Air Pressure Head

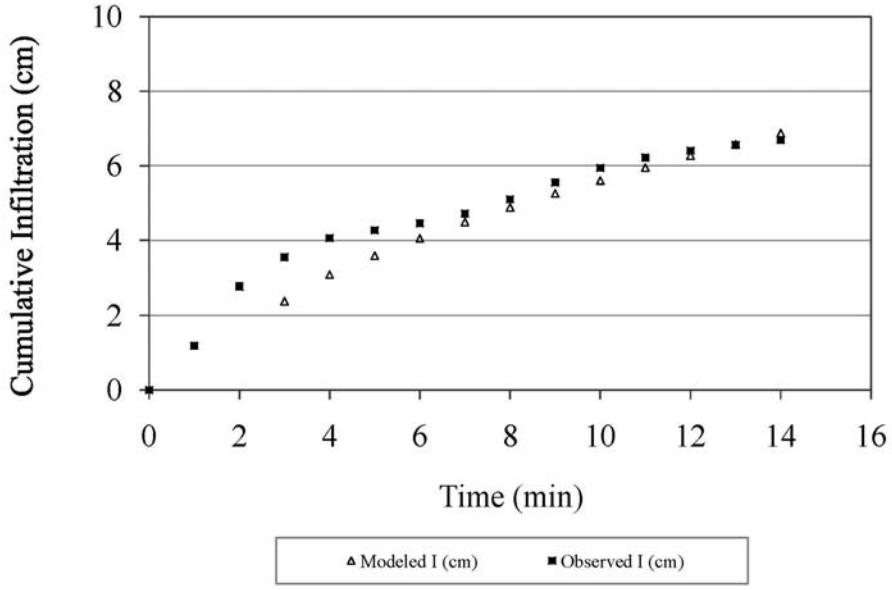

Figure 30: Experiment No. 10 Modeled and Observed Cumulative Infiltration

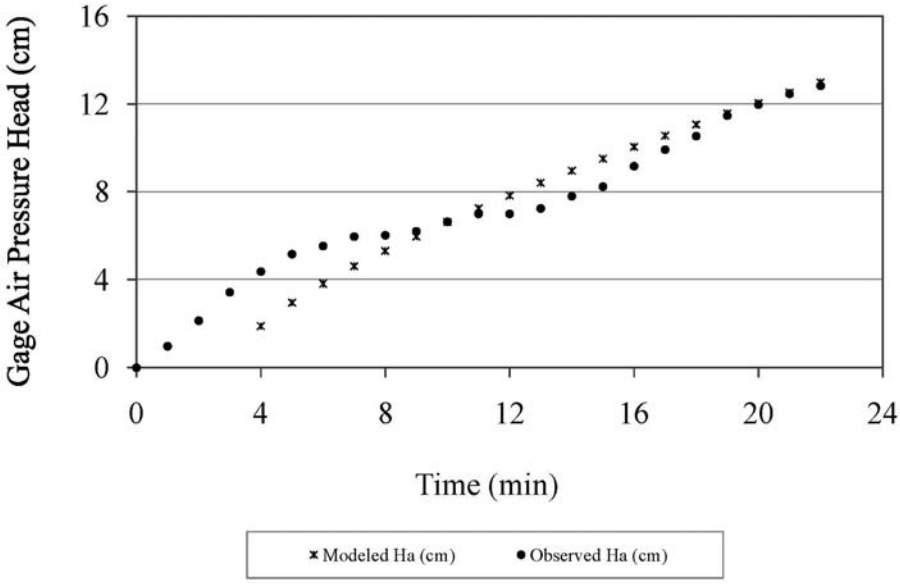

Figure 31: Experiment No. 11 Modeled and Observed Gage Air Pressure Head

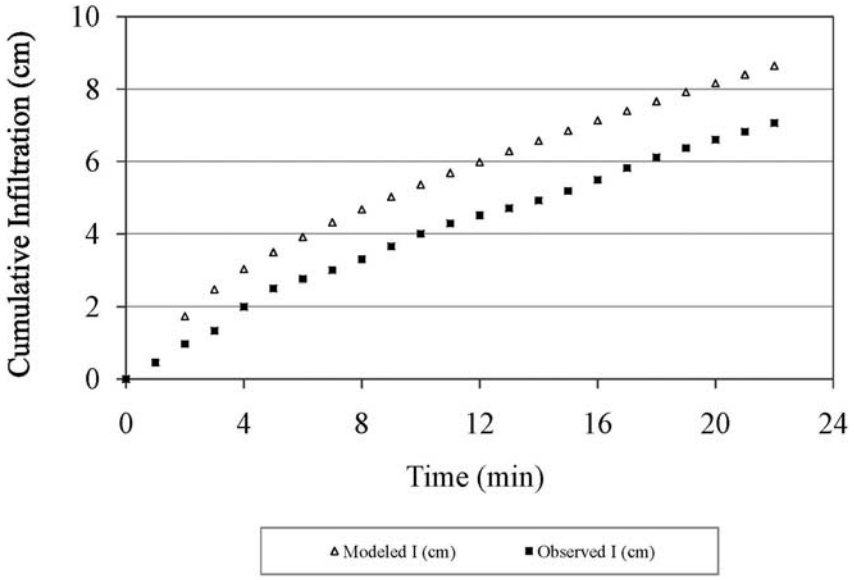

Figure 32: Experiment No. 11 Modeled and Observed Cumulative Infiltration

Figures 15 through 32 show that a better match of modeled cumulative infiltration and gage air pressure values with observed cumulative infiltration and gage air pressure values was obtained during the first and the third sets of the soil column experiments. The second set of the experiments (experiments 5 through 8) provided a poor fit of both gage air pressure head values and cumulative infiltration values. The modeled results of the second series of the soil column experiments overestimated cumulative infiltration values and gage air pressure values. This could be attributed to the fact that in the second series of the soil column experiments, ponding and the ponded head of 1.5 cm on top of the soil column was not rapidly but rather gradually achieved by pouring water through the hose with a “rainfall-like” showerhead. This allowed compressed air to gradually escape the soil column profile as the counterflow of air and resulted in smaller gage air pressure

head values. The first and the third sets of the soil column experiments (experiments 1 through 3 and experiments 10 through 11), where the ponded head of 1.5 cm was rapidly achieved by pouring a large amount of water on top of the soil column, provided an overall better fit of gage air pressure head values and cumulative infiltration values. Experiments 1, 2, 10, and 11 provided an excellent fit of both cumulative infiltration values and gage air pressure head values.

Experiment 11 (see Figure 31) was the only observed soil column experiment with a pronounced oscillatory behavior of gage air pressure head values, attributed to the compressed air escaping as the counterflow of air. As this work suggests the proposed algorithm is capable of modeling a gradual built up of gage air pressure head values rather than an oscillatory behavior. Table 5 summarizes initial parameters of the soil column experiments during which modeled and observed values converged.

Table 5: Summary of Initial Parameters for Converged Experiments

Experiment no.	Date	Depth to the water table (cm)	Initial water content (cm^3/cm^3)	Gage air pressure fit ? (y/n)?	Cumulative infiltration fit? (y/n)
1	06.23.2009	162	0.0614	Y	Y
2	06.30.2009	128	0.0774	Y	Y
3	07.14.2009	103	0.1203	N	Y
4	08.22.2009	61	0.244	N/A	N/A
5	06.02.2010	127	0.0756	Y	N
6	06.08.2010	107	0.1023	Y	N
7	06.11.2010	93	0.1472	N	N
8	06.15.2010	74	0.2033	N	N
9	06.22.2010	61	0.2573	N/A	N/A
10	07.07.2010	144	0.0683	Y	Y
11	07.13.2010	109	0.0987	Y	Y

4.4 Comparison of Infiltration Values of Two Infiltration Models

This section compares observed cumulative infiltration results with results of two infiltration models: an original Green and Ampt (1911) infiltration model and a revised Green and Ampt (1911) infiltration model that accounts for both air compression and air counterflow. Since experiments 1, 2, 3, and 11 provided an excellent fit of cumulative infiltration values of the introduced model with experimentally observed values, the results of these soil experiments were compared to the values obtained using the original Green and Ampt (1911) approach. Figures are shown below.

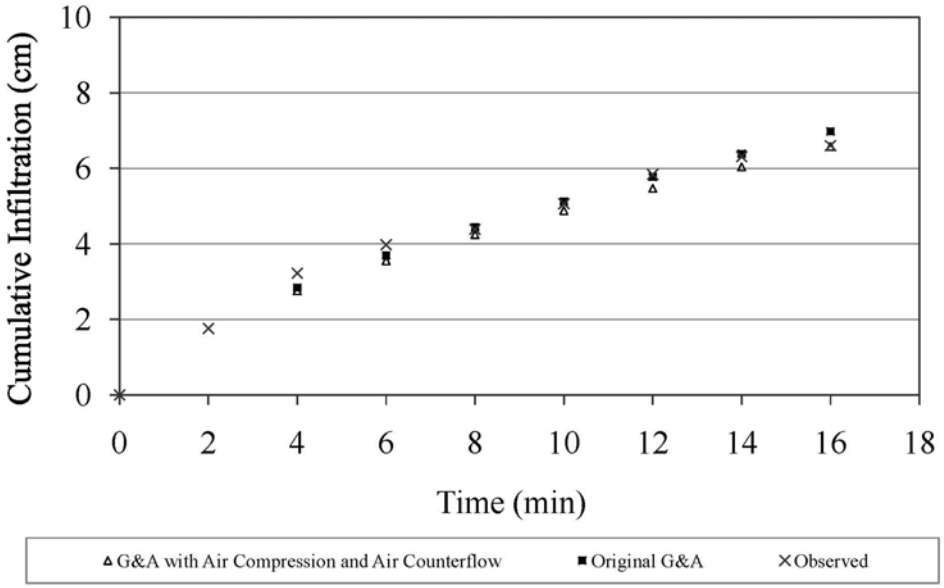

Figure 33: Experiment No.1 Cumulative Infiltration

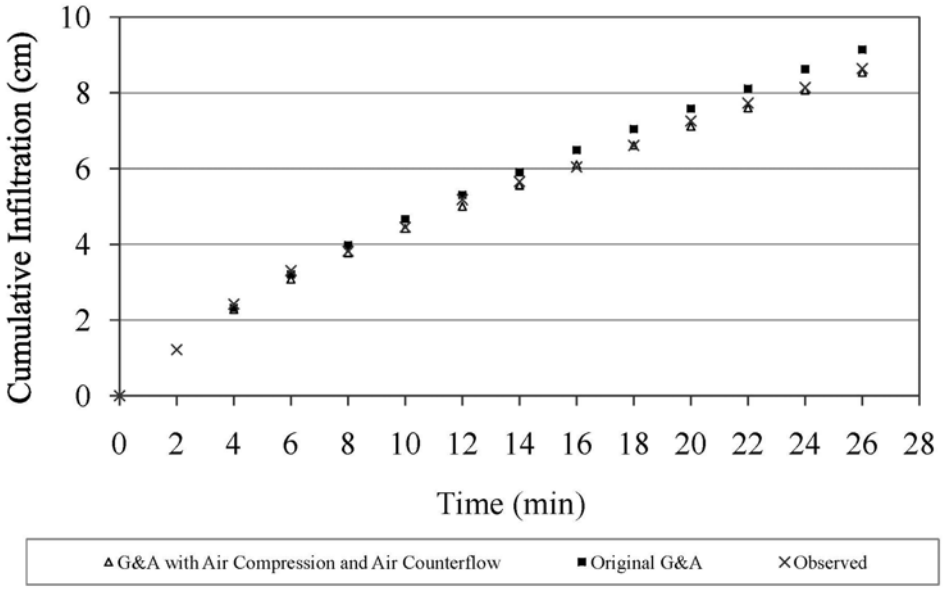

Figure 34: Experiment No.2 Cumulative Infiltration

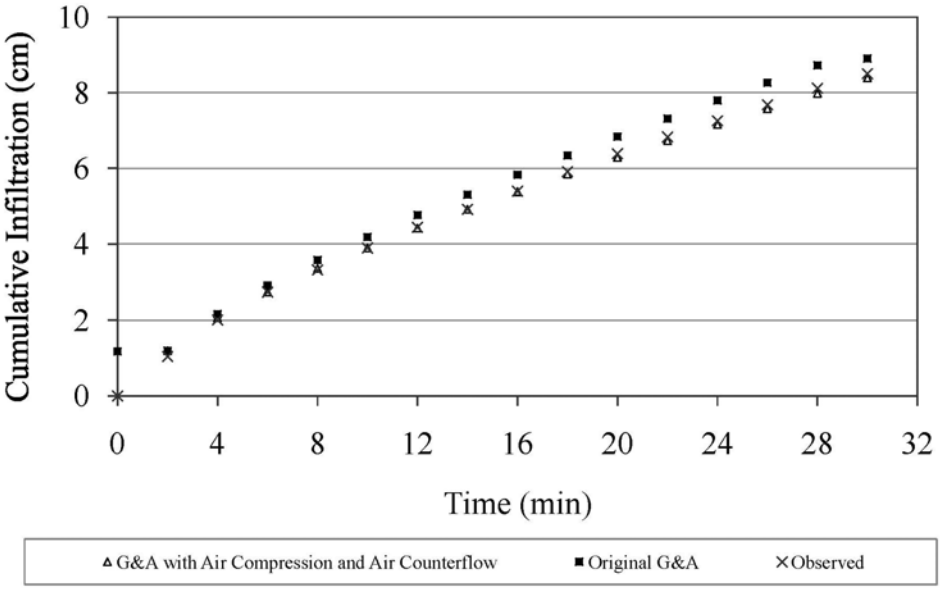

Figure 35: Experiment No.3 Cumulative Infiltration

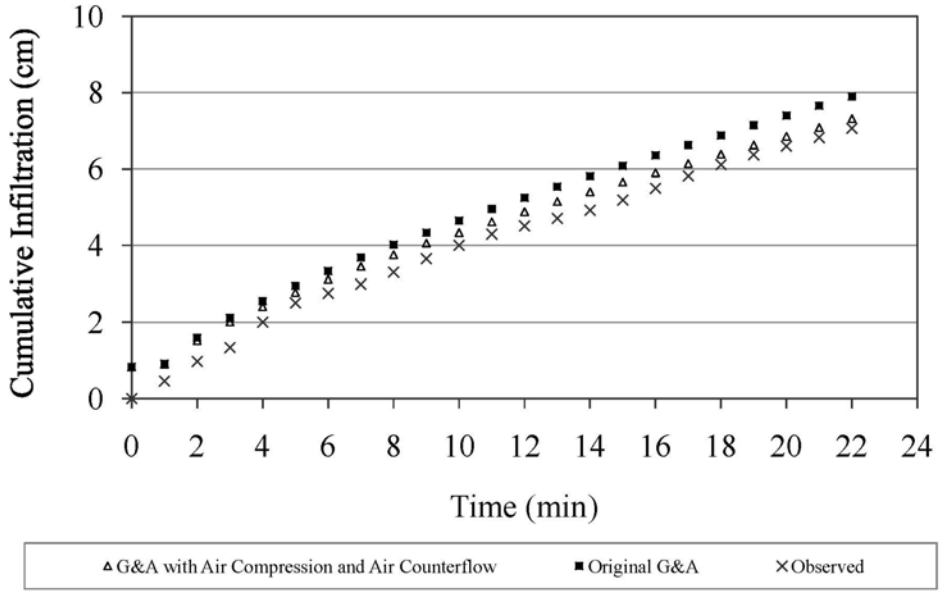

Figure 36: Experiment No.11 Cumulative Infiltration

Figures 33 through 36 suggest that the proposed Green and Ampt (1911) based algorithm provides a better fit of cumulative infiltration values than the values modeled with the original Green and Ampt (1911) infiltration model that does not model air compression or air counterflow.

CHAPTER 5: CONCLUSION

5.1 Summary and Conclusions

Using the results from the laboratory soil column studies a simple set of infiltration equations was tested to predict pressure head build up ahead of the advancing wetting front and cumulative infiltration. Conducted infiltration experiments suggested that cumulative infiltration and infiltration rates depend on the depth to the water table and on the soil water storage capacity. In addition, the infiltration experiments suggested that the air present in the soil of the unconfined aquifer would have an influence on infiltration rates and cumulative infiltration. It was observed that the air present in the soil would bubble up and through the soil surface right after the beginning of infiltration. Secondary effects of air present in the soil, the Lisse effect and its influence on the soil water storage capacity, were also observed during the experiments. It was concluded that the amount of compressed air and hence gage air pressure head readings depend on the antecedent moisture content conditions, depth to the water table, and on the rainfall intensity

Using the basis of the Green and Ampt (1911) approach and Sabeh's (2004) infiltration model air compression and air counterflow was coupled to account for the effect of air compression and air counterflow on infiltration and infiltration rates. Unlike

the original Green and Ampt (1911) model, the revised model accounts for air compression and air counterflow, and unlike Sabeh's (2004) model, air pressure of the remaining air is updated every wetting front depth increment ΔL.

The results show that the introduced model provides a good fit of cumulative infiltration and gage air pressure head values when compared to experimentally observed values. In addition, the proposed model provides a better fit of observed values than the original Green and Ampt (1911) model that overestimates cumulative infiltration. This is due to the fact that the original Green and Ampt (1911) model, unlike the revised model, does not account for air compression or air counterflow.

In general, for certain initial conditions the proposed model fails to match observed gage air pressure head values and cumulative infiltration values and overestimates these values. The model starts simulating gage air pressure head values and cumulative infiltration at the onset of ponding as if water is instantaneously applied. There is no simulation of gage air pressure and infiltration prior to ponding. In reality, if rapidly subjected to a large volume of water, the soil column might have air bubbles trapped and prevented from escaping the soil column but also might have air escaping as a counterflow prior to the soil column reaching ponding conditions. With time these air bubbles slowly dissolve in the soil water and start escaping through the soil surface – this decreases the air pressure developed in the soil column (Hillel 1982).

It can be speculated that the gage air pressure head values were overestimated because the experimental setup was not well suited for simulation of gage air pressure head values given a very large hydraulic conductivity of the soil and a large soil sample.

5.2 Application of the Infiltration Model

Experimental results of this research show that it is important to account for air compression and air counterflow when modeling infiltration. In addition, the proposed model offers an alternate method of estimating infiltration in shallow water table environments with the highly conductive and sandy soils of west central Florida.

This work can be of use to someone studying irrigation techniques of rice or other crops since successful rice irrigation requires maintaining a small constant head above the soil surface which in turn creates air compression between the wetting front and a lower impermeable layer. In addition, this work can serve as a reference to further research dedicated to infiltration into unsaturated zone and effects of air on infiltration in shallow water table environments.

5.3 Shortcomings of the Proposed Method

The revised model provides a good fit of observed cumulative infiltration and gage air pressure head values. However, the model does not always successfully model gage air pressure head and cumulative infiltration values. The model works for certain antecedent soil moisture conditions, depth to the water table conditions, and rainfall conditions. The model appears for work best for the following initial conditions: $\theta_i < 0.1$ cm^3/cm^3 and $D > 1m$.

The proposed infiltration model does not model air compression values ahead of the wetting front during pre-ponding period and starts calculating air compression values

with air counterflow right after the ponding time T_p is reached. This appears to be the reason for overestimating gage air pressure head values.

The proposed model does not describe the infiltration rate. Observed infiltration rates exhibit complex oscillatory behavior that is believed to be due to the counterflowing air escaping through the soil surface. Modeling the oscillatory nature of the infiltration rate and the response of the infiltration rate to air effects requires further research. In addition, the model fails to model cumulative infiltration during periods of little or no rainfall since the main assumption of the model is a constant ponded head on top of the soil column, something that is believed to be achieved and maintained during a high intensity rainfall event. The model does not account for soil variations, crusting effects, initial non-uniform soil moisture contents, or the air entrapment.

REFERENCES

Besbes, M., and de Marsily, G. (1984). "From Infiltration to Recharge: Use of a Parametric Transfer Function." *Journal of Hydrology,* 74, 271-293.

Bouwer, H. (1964). "Unsaturated Flow in Ground-water Hydraulics." *J. Hydraul. Div. Am. Soc. Civ. Eng.,* 90, 121-144.

Brakensiek, D.L. (1977). "Estimating the Effective Capillary Pressure in the Green and Ampt Infiltration Equation." *Water Resour. Res*., 13 (3), 680-682.

Brooks, R. H., and Corey, A.T. (1966). "Properties of Porous Media Affecting Fluid Flow." *J. Irrig. Drain. Div. Am. Soc. Civ. Eng*., 92, 61– 88.

Charbeneau, R. (2000). *Groundwater Hydraulics and Pollutant Transport* , Prentice-Hall inc., 18-90.

Chu, X., and Marino, M.A. (2005). "Determination of Ponding Condition and Infiltration into Layered Soils under Unsteady Rainfall."*Journal of Hydrology* , 313 (3-4), 195-207.

Dunn, A. M, and Silliman, S. (2003). "Air and Water Entrapment in the Vicinity of the Water Table." *Ground Water*, 41 (6), pp. 729-734.

Dunne, T., and Black, R.D. (1970). "Partial Area Contributions to Storm Runoff in a Small New England Watershed." *Water Resour. Res.*, 6(5), 1296–1311.

Durrans, S., Dietrich, K.., Ahmad, M., et al.(2007). *Stormwater Conveyance Modeling and Design*. 1st edition. Bentley Institute Press, Exton, Pennsylvania

Faybishenko, B. (1995). "Hydraulic Behavior of Quasi-Saturated Soils in Presence of Entrapped Air: Laboratory Experiments." *Water Resources Research* , 31(10), 2421-1435.

Free, G.R., and Palmer, V.J. (1940). "Interrelationship of Infiltration, Air Movement, and Pore Size in Graded Silica Sand." *Soil Science Society of America Proceedings*, 5, 390-398.

Green, W.A., and Ampt, G.A. (1911). "Studies on Soil Physics,1. The Flow of Air and Water through Soils," *J. Agr. Sci.,* 4, 1-24.

Grismer, M.E., Orang, M.N., Clausnitzer, V., Kinney, K. (1994). "Effects of Air Compression and Counterflow on Infiltration into Soils." *J. Irrig. and Drain. Engrg*., 120 (4), 775-795.

Hammecker, C., Antonino, C.D., Maeght, J.L., and Boivin, P. (2003). "Experimental and Numerical Study of Water Flow in Soil under Irrigation in Northern Senegal: Evidence of Air Entrapment." European Journal of Soil Science, 54, 491-503.

Heliotus, F.D., and De Witt, C.B. (1987). "Rapid Water Table Response to Rainfall in Northern Peatland Ecosystem. " *Water Resources Bulletin*, 23 (6), 1011-1016.

Hillel, D. (1982). *Introduction to Soil Physics*. Academic Press, New York.

Holtan, H.N. (1961). A Concept for Infiltration Estimates in Watershed Engineering. U.S. Department of Agriculture Bulletin 41-51, Washington, DC, U.S. Department of Agriculture.

Horton, R, E. (1939). "Analysis of Runoff Plot Experiments with Varying Infiltration Capacity." *Transactions, American Geophysical Union*, Part IV, 693-711.

Horton, R.E. (1940). "An Approach toward a Physical Interpretation of Infiltration-Capacity." *Soil Sci. Soc. Am. Proc*. 5, 399-417.

Huggins L.F., and Monke E.J.(1966). *The Mathematical Simulation of the Hydrology of Small Watersheds.* Technical Report No.1, Purdue Water Resources Research Centre, Lafayette.

Hughs, G.M., Landon, R.A., and Farvolden, R.N. (1971). Summary of Findings on Solid Waste Disposal Sites in Northeastern Illinois. Illinois State Geological Survey Environmental Geology Notes, No.45.

Izadi, B., Podmore, T.H., and Seymor, R.M. (1995). "Consideration of Air Entrapment in Surface Irrigation; A Computer Simulation Study."Agricultural Water Management, 28, 245-252.

Klute, A. (1973). "Soil Water Flow Theory and Its Application in Field Situations." *Field Soil Water Regime*. *Soil Sci. Sot. America*, 9-35.

Kostiakov, A.N. (1932). "On the Dynamics of the Coefficients of Water Percolation in Soils." *Sixth Commission, International Society of Soil Science, Part A*, 15-21.

Mein R.G., and Larson, C.L.(1971). *Modeling the Infiltration Component of the Rainfall-runoff process.* WRRC Bull.43, Water Resources Research Center, University of Minnesota, Minneapolis.

Meyboom, P. (1967). "Groundwater Studies in the Assiniboine River Drainage Basin: Part II, Hydrologic Characteristics of Phreatophytic Vegetation in South-Central Saskatchewan." *Geologic Survey of Canada Bulletin*, 139.

Mishra, S.K., Tyagi, J.V., and Singh, V.P. (2003). "Comparison of Infiltration Models." *Hydrological Processes,* 17, 2629-2652.

Morel-Seytoux, H.J. (1973). "Two-phase flow in porous media." *Advances in Hydroscience*, edited by V.T. Chow, 119-202. Academic, San Diego, California.

Morel-Seytoux, H.J., and Khanji, J. (1974). "Deriation of an Equation of Infiltration."*Water Resour. Res.,* 10, 795-800.

Morel-Seytoux, H.J., Meyer, P.D., Nachabe, M., Touma, J., van Genuchten, M.T., Lenhard, R.J. (1996). "Parameter Equivalence for Brooks-Corey and van Genuchten Soil Characteristics: Preserving the Effective Capillary Drive." *Water Resour. Res., 32 (5), 1251-1258.*

Nachabe, M., and Illangasekare, T. (1994). "Use of Tension Infiltrometer Data with Unsaturated Hydraulic Conductivity Models." *Ground Water*, 32(6), 1017-1021.

Nachabe, M., Masek, C., and Obeyesekera, J. (2004). "Observation and Modeling of Profile Soil Water Storage above a Shallow Water Table." *Soil Science Society of America Journal*, 68(3), 719-724.

Overton, D.E. (1964). Mathematical Refinement of an Infiltration Equation for Watershed Engineering. ARS 41-99. U.S. Department of Agricultural Service, Washington, DC.

Peck, A.J. (1965). "Moisture Profile Development and Air Compression during Water Uptake by Bounded Porous Bodies, 2, Horizontal Columns." *Soil Sci*., 99,327-334.

Peck, A. J. (1969). "Entrapment, Stability, and Persistence of Air Bubbles in Soil Water."*Australian Journal of Soil Research* 7, 79–90.

Philip, J.R. (1957). "Theory of Infiltration." *Soil Science*, 83(5), 345-357.

Powers, W. L. (1934) "Soil-water Movement as Affected by Confined Air." *J. A gric. Res*., *49*, 1125–1134.

Rawls, W.J., Brakensiek, D.L., and Miller, N. (1983). Green-Ampt Infiltration Parameters from Soils Data. *Journal of Hydraulic Engineering,* 109 (1), 62-70.

Richards, L.A. (1952). Report of the Subcommittee on Permeability and Infiltration, Committee on Terminology, Soil Science Society of America. *Soil Sci. Soc. Am. Proc.*, 16, 85-88.

Rode, A.A. (1965). *Theory of Soil Moisture, Volume 1.* Published for USDA and NSF by the Israel Program for Scientific Translation, Jerusalem, 1969.

Sabeh, D. (2004) "Adapting the Green and Ampt Model to Account for Air Compression and Counterflow." *A Master Thesis*. Department of Civil and Environmental Engineering. University of South Florida.

Seymour, R.M. (1990). *Air Entrapment and Consolidation as Mechanisms in Infiltration with Surge Irrigation* . Ph.D. Dissertation, Agric. Chem. Eng. Dept., Colorado State University, Fort Collins, CO, 299.

Seymour, R.M. (2000). "Air Entrapment and Consolidation Occurring with Saturated Hydraulic Conductivity Changes with Intermittent Wetting." *Irrig Sci*, 4, 9-14.

Simunek, J., Huang, K., and van Genuchten, M.T. (1998). *The HYDRUS Code for Simulating the One-dimensional Movement of Water, Heat, and Multiple Solutes in Variably-saturated Media, Version 6.0.* Research Report No. 144, US Salinity Laboratory, US Department of Agriculture, Riverside, CA.

Smith. R.E. (1972). "The Infiltration Envelope: Results from a Theoretical Infiltrometer."*Journal of hydrology*, 17, 1-21.

Smith, R.E. , and Parlange J.Y. (1978). "A Parameter-efficient Hydrologic Infiltration Model." *Water Resources Research*, 14 (3), 533-538.

Tindall, J.A., Kunkel, J.R., Anderson, D.E. (1999). *Unsaturated Zone Hydrology for Scientists and Engineers.* Prentice Hall, Upper Saddle River, New Jersey.

Touma, J., Vachaud, G., and Parlange, J.Y. (1984). "Air and Water Flow in a Sealed, Ponded Vertical Soil Column: Experiment and Model." *Soil Science*, 137(3), 181-187.

van Genuchten, M.T. (1980). "A Closed Form Equation for Predicting the Hydraulic Conductivity of Unsaturated Soils." *Soil Sci. Soc. Am. J*., 44,892-898.

Viessman, W., and Lewis, G.L. (2003). *Introduction to Hydrology*. 5th edition. Prentice Hall, Upper Saddle River, New Jersey.

Vomacka, J., Thompson, D., Ross, M., Nachabe, M., and Tara, P. (2002). "Measurement of Surficial Aquifer Recharge, ET, Rainfall, Runoff and Stream-Aquifer Interaction Characteristics of the Central and Southern Region of the Southwest Florida Water Management District." A Field Project Providing Hydrologic Data Collection and Analysis. Center for Modeling Hydrologic and Aquatic Systems Department of Civil and Environmental Engineering, University of South Florida.

Wang, Z, Feyen, J., Nielsen, D., and van Genuchten, M.T. (1997). "Two-phase Flow Infiltration Equations Accounting for Air Entrapment Effects." *Water Resources Research*, 33 (12), 2759-2767.

Wang, Z., Feyen, J., van Genuchten, M., and Nielsen, D. (1998). "Air Entrapment Effects on Infiltration Rate and Flow Instability." *Water Resour. Res*., 34(2), 213-222.

Weeks, Edwin P.. "The Lisse Effect Revisited. (Technical Note)." *Ground Water*. 2002. Retrieved August 08, 2010 from accessmylibrary: http://www.accessmylibrary.com/article-1G1-94775872/lisse-effect-revisited-technical.html.

Whisler, F.D., and Bouwer, H.(1970). "Comparison of Methods for Calculating Vertical Drainage and Infiltration for Soils." *J.* Xuefeng, C., and Mario, M.A. (2005).

Xuefeng, C., and Mario, M.A. (2005). "Determination of Ponding Condition and Infiltration into Layered Soils under Unsteady Rainfall." *Journal of Hydrology*, 313, 3-4, 195-207.

Youngs, E.G., and Peck, A.J. (1964). "Moisture Profile Development and Air Compression during Water Uptake by Bounded Porous Bodies: 1. Theoretical Introduction." *Soil Science*, 98 (5), 290-294.

Zumdahl, S.S., and Zumdahl, S.A. (2003). *Chemistry*. 6th edition. Houghton Mifflin Company, Boston, New York.

APPENDICES

Appendix A: Air and Water Physical Properties at 20ºC

Table 6: Air and Water Physical Properties at 20ºC

	Specific weight (N/m^3)	Density (kg/m^3)	Dynamic viscosity ($N\text{-}s/m^2$)	Kinematic viscosity (m^2/s)
Air 11.81		1.202	1.82*10^(-5)	1.51*10^(-5)
Water 9789		998.2	1.00*10^(-3)	1.00*10^(-6)

Appendix B: Additional Figures

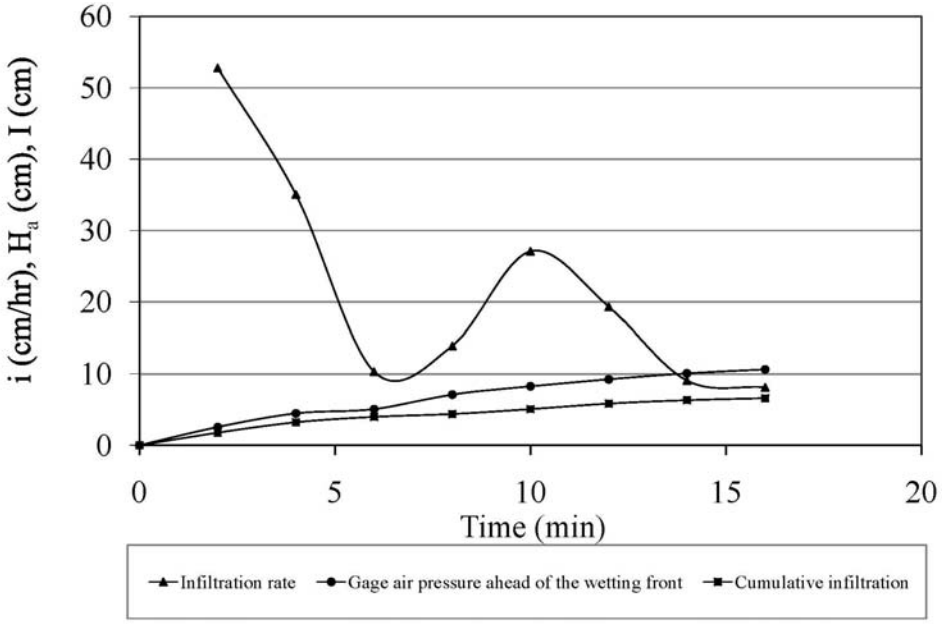

Figure 37: Infiltration Rate, Cumulative Infiltration, and Gage Air Pressure as Functions of Time for Experiment No. 1

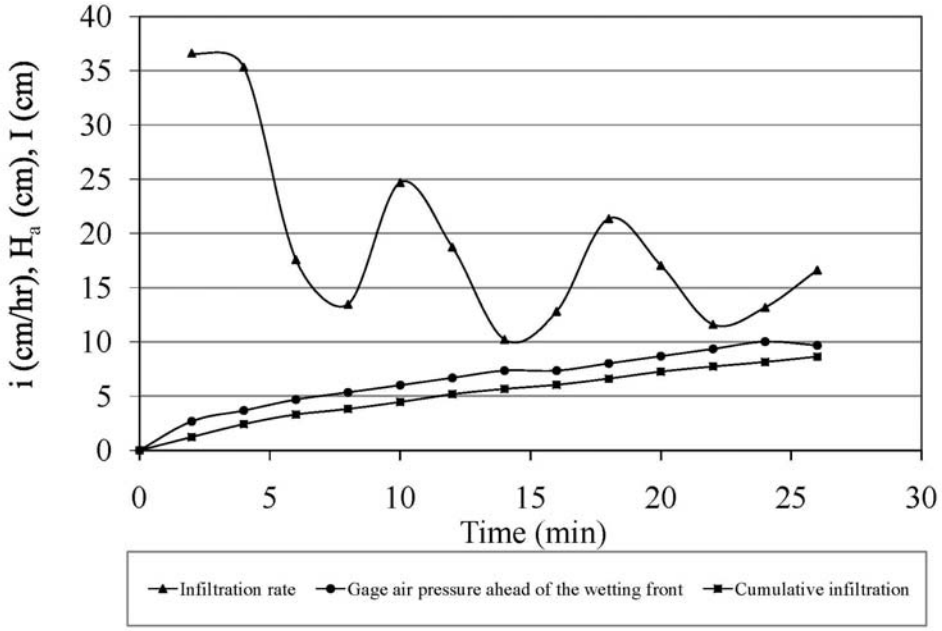

Figure 38: Infiltration Rate, Cumulative Infiltration, and Gage Air Pressure as Functions of Time for Experiment No. 2

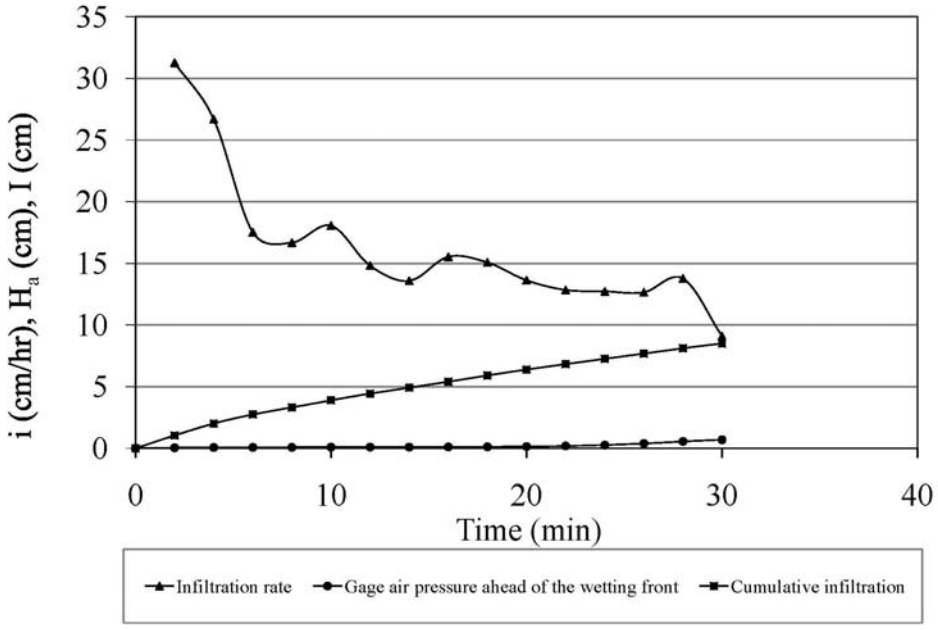

Figure 39: Infiltration Rate, Cumulative Infiltration, and Gage Air Pressure as Functions of Time for Experiment No. 3

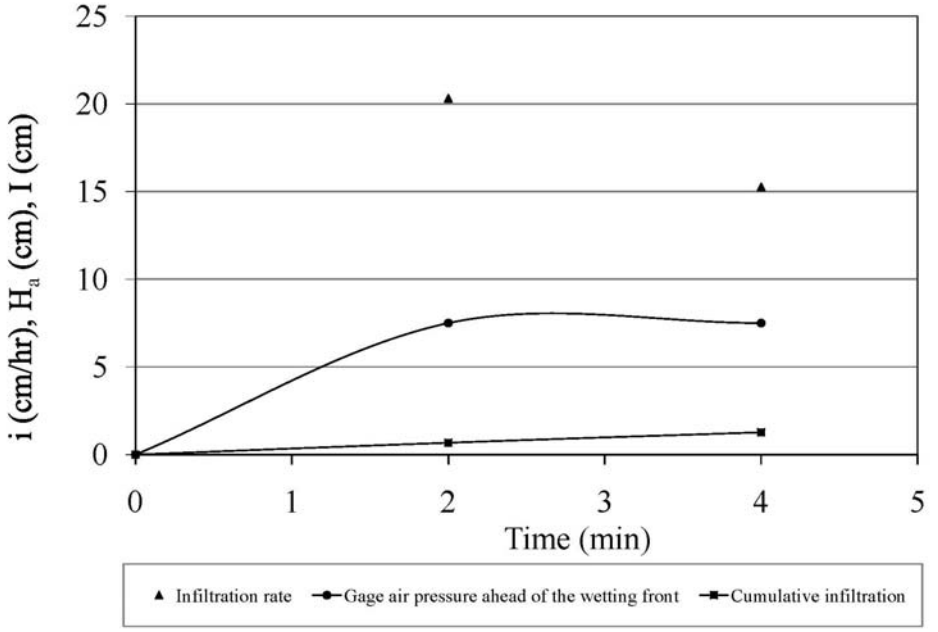

Figure 40: Infiltration Rate, Cumulative Infiltration, and Gage Air Pressure as Functions of Time for Experiment No. 4

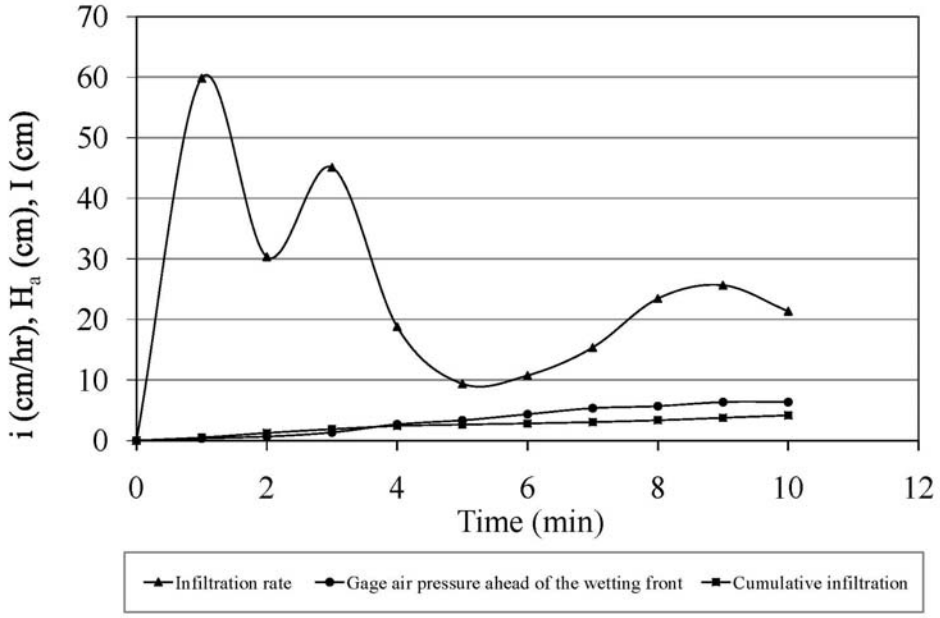

Figure 41: Infiltration Rate, Cumulative Infiltration, and Gage Air Pressure as Functions of Time for Experiment No. 5

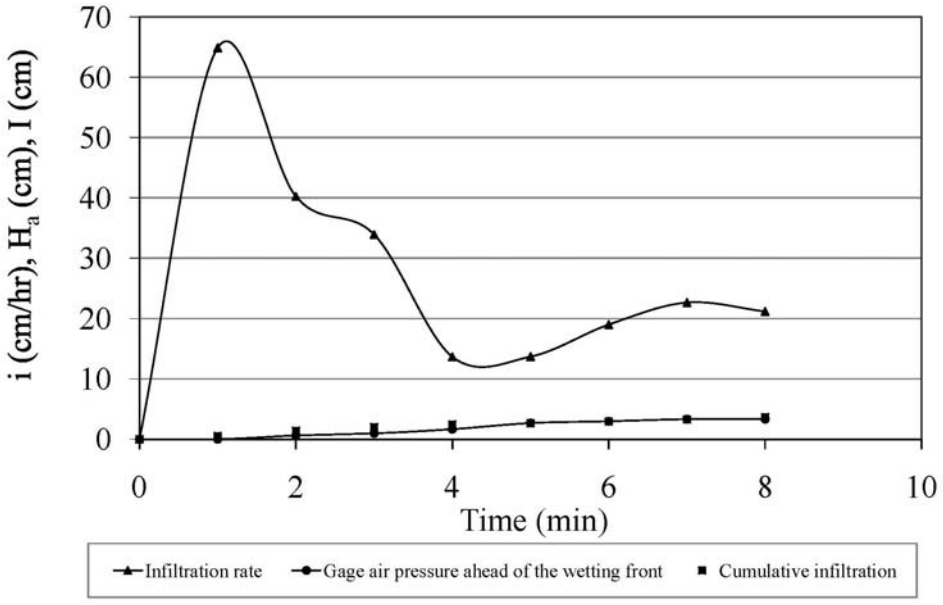

Figure 42: Infiltration Rate, Cumulative Infiltration, and Gage Air Pressure as Functions of Time for Experiment No. 6

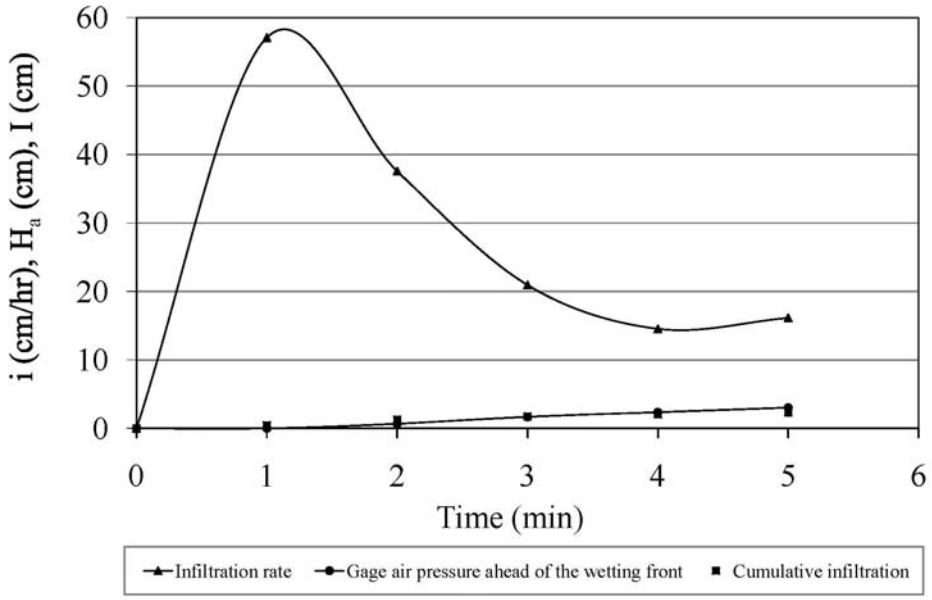

Figure 43: Infiltration Rate, Cumulative Infiltration, and Gage Air Pressure as Functions of Time for Experiment No. 7

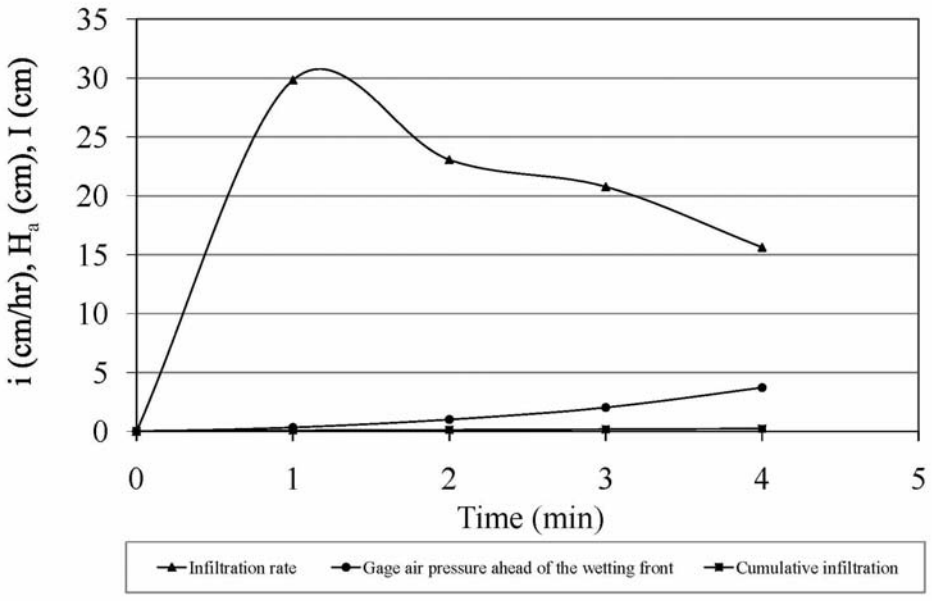

Figure 44: Infiltration Rate, Cumulative Infiltration, and Gage Air Pressure as Functions of Time for Experiment No. 8

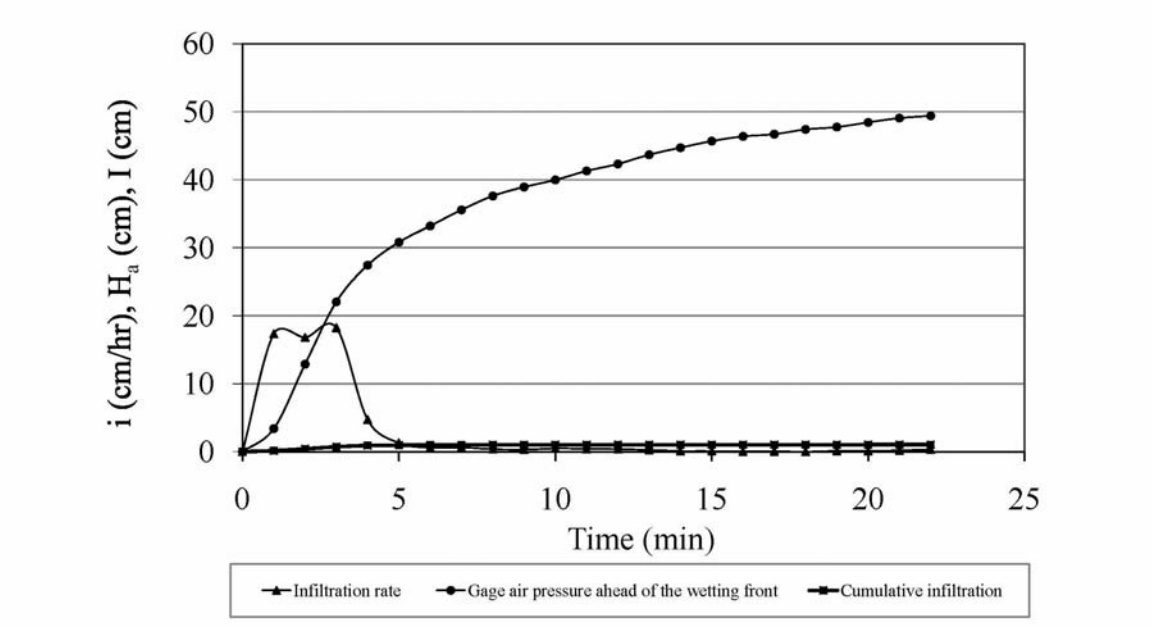

Figure 45: Infiltration Rate, Cumulative Infiltration, and Gage Air Pressure as Functions of Time for Experiment No. 9

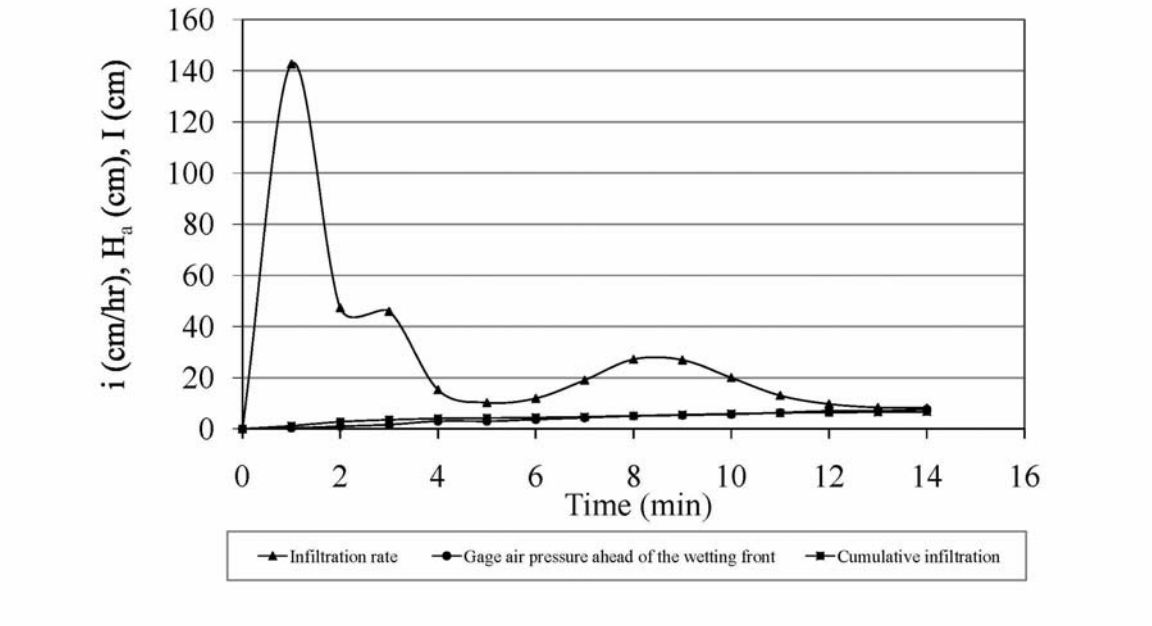

Figure 46: Infiltration Rate, Cumulative Infiltration, and Gage Air Pressure as Functions of Time for Experiment No. 10

Appendix B. (Continued)

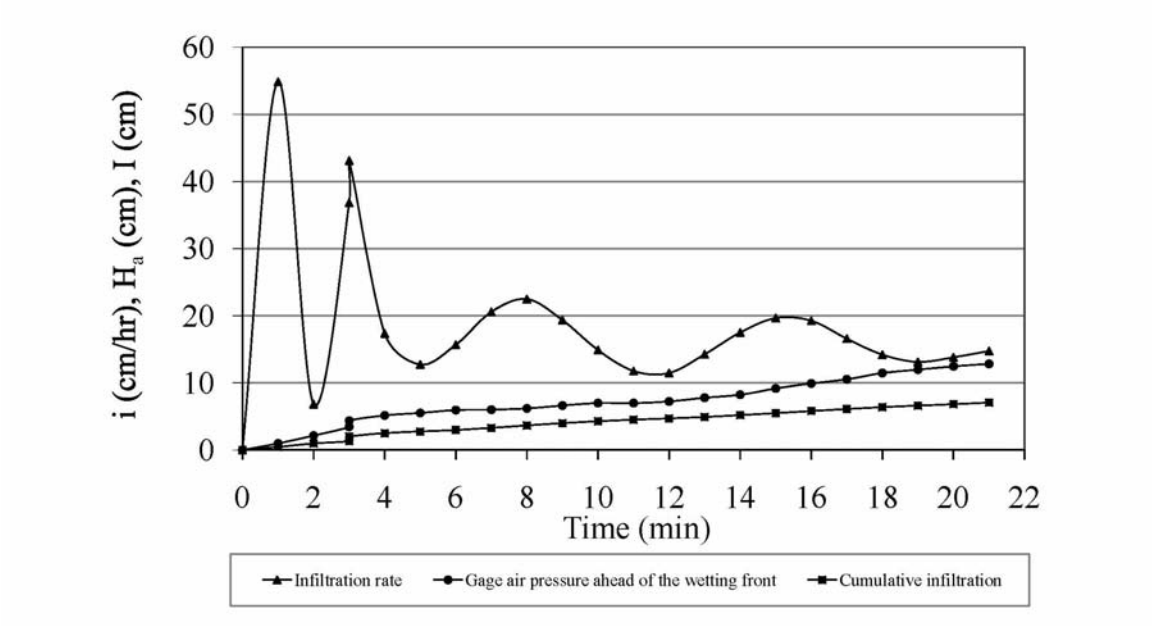

Figure 47: Infiltration Rate, Cumulative Infiltration, and Gage Air Pressure as Functions of Time for Experiment No. 11